Aus der

Neurologischen Universitätsklinik Tübingen

Neurologie mit Schwerpunkt Neurovaskuläre Erkrankungen

# Predicting post-stroke delirium based on TMS-EEG

**Inaugural-Dissertation**

**zur Erlangung des Doktorgrades**

**der Medizin**

**der Medizinischen Fakultät**

**der Eberhard Karls Universität**

**zu Tübingen**

**vorgelegt von**

**Li, Gongfei**

**2026**

Dekanin: Professorin Dr. S. Y. Brucker

1. Berichterstatter: Privatdozentin Dr. A. Mengel

2. Berichterstatter: Professor Dr. M. Giese

Tag der Disputation: 23.04.2026

# Contents

# Figures and tables

## Abbreviation

AEPs ..... auditory evoked potentials

AIC ..... Akaike information criterion

ANCOVA ..... analysis of covariance

ANOVA ..... analysis of variance

AUC ..... area under the curve

CI ..... confidence interval

DAN ..... dorsal attention network

DLPFC ..... dorsolateral prefrontal cortex

DMN ..... default mode network

DWI ..... diffusion-weighted images

EEG ..... electroencephalography

EMG ..... electromyography

ERSP ..... event-related sprectral perturbation

FDI ..... first dorsal interosseous

ICDSC ..... Intensive Care Delirium Screening Checklist

ICA ..... independent component analysis

LCMV ..... linearly constrained minimum variance

MDF ..... median dominant frequency

MEPs ..... motor evoked potentials

MNI ..... Montreal Neurological Institute

MSO ..... maximum stimulator output

NIHSS ..... National Institutes of Health Stroke Scale

NST ..... number of state transitions

PCA ..... principal component analysis

$PCI^{ST}$ ..... fast perturbational complexity index

PIP ..... proximal interphalangeal

PSD ..... post-stroke delirium

RMT ..... resting motor threshold

ROC ..... receiver operating characteristic

ROIs ..... regions of interest

SNR ..... signal-to-noise ratio

SPL ..... superior parietal lobule

STE ..... symbolic transfer entrophy

TFRs ..... time-frequency representations

TMS ..... transcranial magnetic stimulation

TMS-EEG ..... transcranial magnetic stimulation combined with EEG

TEPs ..... TMS-evoked potentials

VLSM ..... voxel-based lesion-symptom mapping

# 1 Introduction

## 1.1 Post-stroke delirium (PSD)

Delirium is a common and severe neuropsychiatric complication of critical illness, potentially arising from diverse underlying causes.(Wilson et al., 2020) Among patients with acute stroke, delirium occurs in approximately 25% of cases, typically within the first 72 hours after stroke onset. (Shaw et al., 2019) The incidence is similar between men and women and increases with advancing age. Its clinical symptoms usually appear within hours to a few days after the stroke event and show considerable fluctuations in both severity and course. PSD is associated with prolonged hospitalization, increased in-hospital and one-year mortality,(Zhang et al., 2024b, McManus et al., 2007) and imposes a substantial burden on both families and healthcare systems.(Gong et al., 2024) Furthermore, by impairing cognitive function, delirium disrupts rehabilitation efforts, hampers functional recovery, and compromises long-term quality of life following discharge.(Bilek and Richardson, 2023, Wilcox et al., 2021)

For PSD, it is considered a multifactorial syndrome caused by the interaction between patient vulnerability and stroke-related precipitating factors.(Regal, 2017) Vulnerability factors include advanced age, preexisting cognitive impairment, frailty, multiple comorbidities, and sensory deficits (hearing or vision loss), with cognitive impairment being the most significant risk factor.(Maldonado, 2008) The stroke event itself and associated acute brain injuries (e.g., large infarcts, intracerebral hemorrhage, cerebral edema) act as major precipitating factors. Additionally, systemic conditions (such as respiratory insufficiency, metabolic or nutritional disturbances, infections, and cardiovascular events), post-stroke environmental stressors (e.g., ICU environment, noise, restricted mobility), and medication use (including sedatives, opioids, benzodiazepines, and certain antipsychotics) can further

increase the risk of delirium. The interaction between these vulnerability and precipitating factors ultimately contributes to the development of PSD.

The pathophysiological mechanisms of delirium are complex and not yet fully understood. Given the numerous precipitating factors and risk factors, as well as the heterogeneous clinical manifestations, it is difficult to explain the onset and progression of delirium through a single pathophysiological mechanism.(Sun et al., 2024) It is likely that multiple mechanisms contribute to its development, including neuroinflammation, neural aging, oxidative stress, neurotransmitter imbalance, neuroendocrine dysregulation, and disturbances in melatonin regulation. These mechanisms may complement each other and partially overlap, ultimately leading to dysregulation of neurotransmission and disruption of neural network connectivity, resulting in a breakdown of system integration and the emergence of delirium symptoms. Among these, the neurotransmitter imbalance hypothesis—such as deficiencies in acetylcholine and melatonin, increased dopamine, norepinephrine, and glutamate, and altered levels of γ-aminobutyric acid, aspartate, or serotonin—plays a central role in the pathogenesis of delirium and serves as the theoretical basis for pharmacological interventions.(Maldonado, 2013)

Delirium is characterized by an acute or subacute disturbance of attention and consciousness, which can manifest as impairments in the content of consciousness, such as decreased attention and disorientation, and impairments in the level of consciousness, such as altered arousal. Patients may also exhibit language disturbances, perceptual and behavioral abnormalities, and other cognitive deficits. The condition typically presents with a fluctuating course, developing over hours to several days. Patients often experience disorientation to their environment and, at times, to their own personal information such as name, age, or occupation. Consciousness may be reduced, presenting as apathy, drowsiness, or decreased alertness, or excessively increased, with hypervigilance, irritability, agitation, aggression,

and refusal to cooperate with medical care. Cognitive impairments may include perceptual disturbances such as illusions or hallucinations, memory and learning deficits, impaired abstract thinking and comprehension, executive dysfunction (including the ability to set goals, plan, implement, and adjust actions), and language deficits. Additionally, delirium is often accompanied by disturbances in biological rhythms and emotional regulation, characterized by disrupted sleep-wake cycles, sleep inversion, fear, irritability, agitation, and anxiety, reflecting the complex and multifaceted nature of the syndrome.(Mattison, 2020)

Based on different levels of motor activity, PSD can be classified into three motor subtypes: hypoactive (accounting for 21.7% of cases), hyperactive (10.5% of cases), and mixed (alternating between hypoactive and hyperactive, 67.8% of cases).(Mengel et al., 2021) Hypoactive delirium is characterized by lethargy and fatigue, whereas patients with hyperactive delirium often exhibit agitation and resist cooperation with medical and nursing staff.

Currently, several delirium screening tools are available, including the Confusion Assessment Method (CAM), its modified version for critically ill patients (CAM-ICU), the Intensive Care Delirium Screening Checklist (ICDSC), the 4 A's Test (4AT), the Nursing Delirium Screening Scale (Nu-DESC), and the Delirium Observation Scale (DOS).(Chen et al., 2021) Each of these tools has its own advantages and limitations when applied to stroke patients. Delirious states typically emerge within the first 72 hours after stroke, with the risk gradually declining thereafter. Up to 92% of delirium cases can be identified within the first seven days of hospital admission. It is important to note that environmental changes can also trigger delirium, for example, when patients are transferred between stroke unit and a rehabilitation ward or a general ward. Therefore, continuous delirium screening is usually recommended during the first 5–7 days after admission and within 24–48 hours after transfer.

Delirium can be diagnosed according to the criteria of either the DSM-V or the International Classification of Diseases, Tenth Revision (ICD-10). A DSM-V-based diagnosis of delirium requires the following criteria to be met: (A) disturbance in attention and awareness; (B) an acute onset with fluctuating course; (C) disturbance in cognition; Criteria D and E relate to exclusion of alternative explanations for the disturbances in criteria A and C, such as other neurocognitive disorders (D) or medical conditions, drug use or withdrawal or toxin exposure (E).(Wilson et al., 2020) Compared to DSM-V, ICD-10 diagnostic criteria require the presence of at least one additional feature, such as a sleep–wake rhythm disturbance (e.g., sleep disruption, worsening symptoms at night, or hallucinations upon awakening). The vast majority of clinical studies rely on DSM-V for diagnostic assessment; consequently, DSM-V is widely regarded as the gold standard for delirium evaluation.(Stollings et al., 2021)

The treatment of delirium primarily relies on non-pharmacological interventions, which are especially recommended for hypoactive delirium. These interventions include environmental optimization, maintaining regular routines, cognitive stimulation, and pain management. Pharmacological treatment is considered only when non-drug measures are ineffective or in cases of severe behavioral or emotional disturbances, risk to self or others, or interference with necessary medical care. The main goals of drug therapy are sedation and control of agitation and psychotic symptoms. Commonly used medications include haloperidol, quetiapine, olanzapine, and risperidone. Since pharmacological treatments have limited efficacy and may be associated with adverse effects, the primary focus of delirium management should remain on identifying and addressing precipitating factors and implementing non-pharmacological interventions.(Mattison, 2020)

## 1.2 Transcranial magnetic stimulation combined with Electroencephalography (TMS-EEG)

Transcranial magnetic stimulation (TMS) is a non-invasive method for investigating neurophysiological activity in the human brain. The combination of TMS with electroencephalography (EEG) enables the design of experiments to non-invasively investigate brain states, both in motor and non-motor areas, including the dynamics of cortical interactions on the millisecond timescale, mechanisms of normal and abnormal plasticity, and the interplay between excitatory and inhibitory processes.(Tremblay et al., 2019) By recording TMS-evoked potentials (TEPs) and TMS-induced cortical oscillations, TMS-EEG is no longer restricted to the analysis of the primary motor cortex but can be applied to assess brain function across nearly all cortical regions and their associated networks. Early attempts to record EEG signals during magnetic stimulation were hampered by severe electromagnetic and myogenic artifacts; however, the development of TMS-compatible EEG systems has largely resolved these issues. Furthermore, various methods, including independent component analysis, can be applied to remove artifacts arising from environmental noise and physiological sources (e.g., cardiac activity, eye blinks, head movements, and craniofacial/ scalp muscle activity), as well as artifacts directly related to TMS.(Hernandez-Pavon et al., 2023)

A TMS pulse applied to the cortex triggers time-locked neuronal depolarization and trans-synaptic activation of both local and distant cortical networks.(Paparella et al., 2023) Scalp EEG electrodes can record this activity, where the summed postsynaptic potentials appear as alternating positive and negative deflections, referred to as TMS-evoked potentials. Depending on the site of stimulation, TEPs exhibit stereotypical patterns of alternating negative and positive deflections, which facilitates the application of TMS-EEG in research. Additionally, TMS-EEG can be employed to investigate the distinct

roles of brain rhythms and to probe thalamocortical circuits by directly measuring TMS-induced oscillatory activity resulting from phase resetting. This provides a unique opportunity to quantify frequency-specific activity directly elicited by TMS pulses, described as transient phase alignment of oscillatory activity. In this way, TMS-EEG allows the investigation of the natural or resonant frequency of specific brain regions, reflected in short-lived neuronal synchronization at particular frequencies following stimulation. TMS-EEG research can be conducted not only at the sensor level but also at the source level, through source reconstruction methods, thereby enhancing spatial resolution and enabling clearer cortical visualization with the aid of anatomical atlases.

Currently, TMS-EEG is applied not only in studies of healthy populations but also extensively across a wide range of neuropsychiatric disorders, including schizophrenia, depression, bipolar disorder, stroke, Alzheimer's disease, epilepsy, and Parkinson syndrome.(Tremblay et al., 2019) It holds significant clinical relevance for the prevention, treatment, and mechanistic understanding of these conditions. TMS-EEG has emerged as a powerful tool, enhancing our capacity to investigate brain function non-invasively across health and disease, while offering objective, quantifiable, and reproducible measures into neuronal excitability, inhibition, oscillatory dynamics, connectivity, and plasticity.

## 1.3 Objective and Hypothesis

Accurate identification of individuals at high risk for PSD—prior to its onset—is of critical importance. It may enable the implementation of targeted strategies to prevent its occurrence or attenuate its severity.(Kneihsl et al., 2024) Although previous studies have investigated clinical risk factors and candidate biomarkers for PSD, predictive accuracy has remained limited, and data of effective intervention strategies based on these markers are lacking.(Siokas et

al., 2022, Zhang et al., 2024a, Mukminin et al., 2025, Alvarez-Perez and Paiva, 2017, Oldenbeuving et al., 2014) Reasons for this still unsatisfactory situation may be the etiological diversity of delirium, its broad array of precipitating factors, and the complexity of its underlying pathophysiology. Moreover, as most studies have focused on clinical indicators, it remains challenging to identify a single representative and mechanistically informative predictor.

Growing evidence suggests that delirium arises from dysfunction in large-scale brain networks.(Maldonado, 2018, van Montfort et al., 2019) This concept proposes that diverse etiologies and precipitating factors converge on common network-level disruptions, ultimately producing the clinical phenotype of delirium. Characteristic features of disturbed brain network dynamics include reduced functional connectivity between key nodes, decreased complexity of brain activity, and imbalance between functional networks—particularly the default mode network (DMN) and dorsal attention network (DAN)—contributing to core symptoms such as inattention and perceptual disturbance.(Eeles et al., 2017) These patterns have been confirmed in multiple EEG and neuroimaging studies.(Hanna et al., 2023, Boukrina and Barrett, 2017, Boukrina et al., 2022, van Montfort et al., 2018) Identifying a universal neurophysiological marker that captures this large-scale brain network dysfunction may therefore offer promising predictive utility.

As a novel technique, TMS–EEG enables the direct assessment of both local and distributed cortical dynamics.(Hernandez-Pavon et al., 2023) By capturing TMS-evoked potentials and induced oscillations, it provides insight into cortical excitability and response signal complexity.(Tremblay et al., 2019) Unlike resting-state EEG, TMS–EEG offers temporally precise and externally driven measurements of cortical reactivity. Previous studies have successfully applied TMS–EEG in the investigation of various neuropsychiatric disorders.(Cao et al., 2021, Julkunen et al., 2022, Li et al., 2021, Strafella et al., 2022, Nardone et al., 2021) We will primarily investigate the predictive value of fast perturbational

complexity index ($PCI^{ST}$) for delirium risk, which is a novel index of brain network complexity that assesses the capacity of thalamo-cortical circuits to engage in complex causal interactions.(Comolatti et al., 2019) It has been validated as a reliable and accurate measure for detecting consciousness, and compared to the traditional PCI, it is simpler and faster to compute, offering promising clinical applicability.

In our earlier study, stimulation was restricted to the right hemisphere, because it has been reported that damage to right-hemispheric cortical and subcortical attention and arousal networks plays a critical role in the development of delirium.(Boukrina and Barrett, 2017) However, growing evidence suggests that delirium involves more widespread brain network abnormalities. Meanwhile, we also aim to examine the interaction between lesion laterality and stimulation side in predicting delirium with TMS-EEG. Therefore, we extend this approach by applying bilateral TMS–EEG to examine whether reductions in perturbational complexity independently predict PSD, irrespective of lesion laterality.

# 2 Material and Methods

## 2.1 Study design

The DELIRISK2 study is a clinical study that prospectively collects patient data from the University Hospital of Tübingen and was designed and conducted by the Department of Neurology with a focus on neurovascular diseases. Following approval (ethics number 147/2020BO1) by the Ethics Committee of the University Hospital of Tübingen, patients who had suffered an acute stroke were examined in their own patient room using a mobile TMS-EEG in order to gain knowledge about the prediction of PSD using TMS-EEG.

## 2.2 Participants

We recruited 34 stroke patients on the stroke unit at Tübingen University Hospital. Inclusion criteria were: (1) age over 50 years, to focus on a representative stroke population; (2) confirmed diagnosis of acute ischemic or hemorrhagic stroke (patients with symptoms of neurological deficits lasting more than 24 hours), including both supratentorial and infratentorial strokes; (3) enrollment at early stage within 48 hours of stroke onset; and (4) informed consent obtained from the patient. Exclusion criteria were: (1) current delirium, or a history of delirium, seizures, or traumatic brain injury within the past three months; (2) contraindications for TMS (e.g., pacemaker, epilepsy)(Rossi et al., 2021); (3) use of central nervous system stimulants or depressants within one week; and (4) inability to elicit motor evoked potentials (MEPs) in contralesional motor cortex (M1) even at maximum TMS intensity.

All experimental procedures are done bedside in the stroke unit. Five-minute resting-state EEG and TMS-EEG recordings from four targets were obtained first, followed by delirium assessments every 8 hours by experienced nurses. Demographic data (gender, age), lesion location, presence of aphasia, and

National Institutes of Health Stroke Scale (NIHSS) score at the time of measurement were documented. In six patients, 3D MPRAGE T1 MRI could not be acquired, and a Montreal Neurological Institute (MNI) standard MRI (MNI ICBM152 non-linear symmetric T1 Average Brain) was used for TMS navigation. The study was approved by the Ethics Committee of Tübingen University Hospital, and performed in accord with the Declaration of Helsinki.

## 2.3 MRI acquisition

High-resolution T1-weighted whole-brain anatomical MRI (3D MPRAGE, 176 sagittal slices, matrix size: 256 × 256, voxel size: 1 × 1 × 1 $mm^3$, TR: 1800 ms, TE: 2.5 ms, duration: 4 min 18 s) was acquired on a Siemens 3 Tesla Tim Trio scanner for patients. Diffusion-weighted images (DWI) (TR: 3900 ms, TE: 95 ms, FOV: 230 mm, 22 axial slices, voxel size: 1.8 × 2.99 × 6 $mm^3$) were also collected during routine clinical imaging.

## 2.4 TMS-EEG preparation

Before starting data collection, we transferred the patients from their beds in the stroke unit to the rehabilitation chairs, a process that usually requires the assistance of a caregiver or physiotherapist because many patients have limited mobility or other neurological deficits. We prepared pillows and cushions to ensure that the patient remained comfortable during the experiment. We informed the patient before the experiment that we would terminate the experiment at any time if there was any discomfort. We placed the rehabilitation chair as far away as possible from other electronic equipment in the ward. TMS-EEG data were recorded using a TMS-compatible EEG system (BrainAmp 64 actiCHamp Plus, BrainProducts GmbH, Munich, Germany). The EEG cap was equipped with TMS-compatible C-ring slit Ag/AgCl electrodes in the

International 10–20 system. To ensure that the EEG cap was worn in accordance with the requirements, we measured the distance on the surface of the scalp between nasion and inion, as well as the distance between the left and right preauricular points, and the reference electrode, Cz, was arranged at the position of the intersection of the two lines (50% of the length). The EEG activity detected by the scalp electrodes is itself very weak, so the scalp needs to be treated first to minimize the resistance. Under each electrode we parted the hair to expose the scalp, then exfoliated the scalp surface with a cotton swab dipped in a scrub, and finally filled the gap between the electrode and the scalp with a conductive gel. We can make several adjustments to ensure that the impedance at all electrodes was kept below 5 kΩ. We then covered the EEG cap with plastic film to protect the filled conductive gel and secured it with an elastic head cap. We used scissors to cut the sides of the elastic head up to expose the external auditory canal, and the patient was given earplugs to reduce the effects of ambient noise and TMS click. We chose earplugs but not noise masking for TMS-EEG recording because long-time exposure to high-decibel white noise was not tolerable for most of the acute stroke patients and even induced delirium. The electrodes in the EEG cap were connected to an electrode input box via cables, each containing two connectors, and the input box was further connected to the EEG amplifier by cables. The EEG amplifier was configured with a DC to 1 kHz hardware filter and a 5 kHz sampling rate, which was powered by a portable battery. To record motor-evoked potentials (MEPs) elicited by TMS, surface electromyography (EMG) electrodes (Ag–AgCl cup electrodes) were placed on the subject's ipsilesional hand. One electrode was positioned over the relaxed first dorsal interosseous (FDI) muscle, and the other electrode was placed in a belly-tendon configuration, approximately at the level of the proximal interphalangeal (PIP) joint of the index finger. EMG electrodes are also connected to the input box via cables.

## 2.5 Individual resting motor threshold (RMT)

After all parts were properly set, a brief screening test was conducted to verify whether MEPs could be elicited in the ipsilesional hand muscles through TMS. The TMS pulses were generated using a MagVenture stimulator (MagPro Compact, MagVenture A/S, Denmark) equipped with a figure-of-eight coil (C-B60, MagVenture A/S, Denmark). The coil was activated and positioned over the motor cortex of the contralesional hemisphere. By pressing the button on the coil, the cortex could be magnetically stimulated, ideally eliciting an action potential at the lowest possible stimulation intensity. The resulting action potential was recorded via electrodes placed on the hand muscles and displayed using the BrainVision Recorder. Participants in whom no action potential could be elicited even at the maximum stimulation intensity were considered unsuitable for the subsequent TMS-EEG experiment, and the testing was terminated at this point. For participants in whom an action potential could be elicited, the individual RMT of the contralesional M1 was determined by recording MEPs from the contralateral FDI muscle during spontaneous relaxation. Surface EMG was recorded using Ag-AgCl cup electrodes placed in a belly-tendon configuration. The raw EMG signal was amplified, band-pass filtered (20 Hz to 2 kHz), and digitized at a sampling rate of 10 kHz via the AUX channel of the amplifier (BrainAmp 64 actiCHamp Plus, BrainProducts GmbH, Munich, Germany) and a BIP2AUX adapter (BrainProducts GmbH, Munich, Germany). The individual RMT was determined as the lowest stimulation intensity capable of eliciting a peak-to-peak MEP exceeding 50 μV in at least 5 of 10 consecutive trials.(Rossini et al., 2015) Importantly, the individual RMT is always determined at the "motor hotspot," rather than using the hand motor region defined in the neuronavigation system based on T1-weighted anatomical images. During the search for the cortical representation area ("motor hotspot"), the position and orientation of the coil are adjusted to elicit the largest MEP response.

## 2.6 Resting-state EEG

After the participant was prepared, a 5-minute resting-state EEG (64 channels, see above) was recorded. During this procedure, it was ensured that the participant remained calm and relaxed with eyes open while sitting in the rehabilitation chair. The EEG was recorded using the BrainVision Recorder system.

## 2.7 Neuronavigation

A stereotactic neuronavigation system (Localite GmbH, St. Augustin, Germany) was employed, using individual anatomical MRI scans to accurately position the TMS coil relative to the participant's brain anatomy. To determine the standardized localization of TMS targets, each participant's brain was aligned to a template based on the MNI coordinate system, referencing the anatomical locations of the anterior and posterior commissures and a point on the falx cerebri. Based on prior findings showing TMS-EEG differences between PSD and non-PSD groups when stimulating the right dorsolateral prefrontal cortex (DLPFC) and superior parietal lobule (SPL),(Bai et al., 2023) we selected bilateral DLPFC and SPL as stimulation targets. These were localized using MNI coordinates (left DLPFC: x = -41, y = 41, z = 16; right DLPFC: x = 42, y = 44, z = 14; left SPL: x = -15, y = −71, z = 52; right SPL: x = 19, y = −69, z = 54). Prior to stimulation, an experienced neurologist assessed the relationship between the stimulation targets and the stroke lesion based on imaging findings, ensuring that the distance between the stimulation site and the lesion was greater than 2 cm to avoid any interference from the lesion itself on the stimulation effects.(Sarasso et al., 2020, Gosseries et al., 2015) First, the stimulator and laptop were turned on, and the participant's MRI DICOM images, provided by radiology on a CD, were saved to an external drive (USB). This

drive was connected to the Localite laptop, and the TMS-Navigator software was opened. On the left side of the display, the toolbar was used to select the participant folder, and upload the DICOM images. Next, brain segmentation was performed: a point in the white matter was marked in the 3D brain image and “Calculate” was clicked, displaying the brain in red for easier identification of structures, which means brain tissues were segmented from skull and scalp. Then, the Talairach definition was performed. To determine the standardized localization of TMS targets, each participant's brain was aligned to a template based on the MNI coordinate system, referencing the anatomical locations of the anterior and posterior commissures and a point on the falx cerebri. The grid boundaries could be adjusted to encompass the entire cerebrum. Afterwards, MNI planning was carried out, and the target structures for stimulation were marked. On the right side of the display, the standard planning mode and “Target” tab were selected. Rotation angles were set to 315° for right DLPFC, 45° for left DLPFC, 345° for right SPL, and 15° for left SPL. This generated the corresponding points on the scalp for each target. Next, patient registration was performed by selecting it from the left toolbar. Three points— nasion, left and right preauricular points— were marked to provide reference points to the software. At this stage, planning was complete and navigation could begin. Navigation was essential to project the software-marked reference points and stimulation targets onto the participant’s scalp to ensure optimal coil positioning. The participant sat in the rehabilitation chair near the Localite laptop and camera, with a forehead reference tracker attached. Using the Localite system pointer, the three registered points (nasion, left and right preauricular points) were sequentially marked on the head and fixed with a blue foot pedal once aligned. To register additional scalp points, the pointer was placed on the head while holding the blue pedal, moving in multiple directions across the scalp. Finally, before stimulation, the four targets (bilateral DLPFC and SPL) were located on the scalp. At this point, all necessary settings and preparations were completed, and stimulation commenced.

## 2.8 TMS-EEG recording

The operator stood next to the participant, holding the figure-of-eight coil and positioning its center over the target site for stimulation. We used a stimulation intensity of 90% RMT, delivering 120 single-pulse stimuli with a 2-second interval between each stimulation (bilateral DLPFC and SPL). The ordering of targets followed a pseudo-random scheme and was balanced between patients. The EEG software Brain Vision Recorder was started to record, after which stimulation was conducted. After stimulating one target, the EEG recording was stopped, the coil was repositioned to the next target, and recording and stimulation were resumed. The optimal coil orientation could be adjusted according to the neuronavigation system. After all four target sites were stimulated, the elastic head cap, EEG cap, and plastic film were removed, the EMG electrodes on the participant's hand were taken off, and the conductive gel on the head was cleaned. At this point, the TMS-EEG data acquisition was completed.

## 2.9 Delirium assessment

Delirium was assessed every 8 hours over 7 days using the Intensive Care Delirium Screening Checklist (ICDSC), validated for stroke unit and ICU settings.(Devlin et al., 2018, Barr et al., 2013) The scoring was performed by experienced nurses at Tübingen University Hospital. Eight clinical features were assessed: level of consciousness, inattention, disorientation, hallucinations and delusions, psychomotor activity, speech, sleep-wake cycle, and symptom fluctuation, with each feature scored as 0 (not present) or 1 (present). For patients without aphasia symptoms, a score of 4 or higher on the ICDSC was considered indicative of delirium. For patients with aphasia

symptoms, a score of 5 or higher on the ICDSC was considered indicative of delirium. Ultimately, an experienced neurologist, independent of the ICDSC scores and TMS-EEG analysis results, used the DSM-V diagnostic criteria to assess whether the patient had delirium. Based on the assessment results, patients were classified into two groups: PSD and non-PSD group. During this period, responsible medical staff regularly assessed and documented NIHSS scores.

## 2.10 Data analysis

### 2.10.1 Resting-state EEG preprocessing

Resting-state EEG data were preprocessed using MATLAB (2023b, MathWorks Inc., Natick, USA) and EEGLAB 2024.0. A zero-phase FIR filter (1–100 Hz) and a 48–52 Hz notch filter were used to remove 50 Hz power-line noise. The EEG data were then downsampled from 5 kHz to 1 kHz. Bad channels were identified through automated and manual inspection and then interpolated using signals from neighboring channels, while noisy epochs were manually rejected, thereby ensuring the quality of the EEG data used for further analysis. Independent Component Analysis (ICA) was performed to remove ocular and stereotypical artifacts based on visual inspection of independent components. Finally, the data were re-referenced to the average reference to minimize reference bias.

### 2.10.2 TMS-EEG preprocessing

Preprocessing of TMS-EEG data was conducted using custom MATLAB scripts (Version 2023b, MathWorks Inc., Natick, USA) in combination with EEGLAB 2024.0. The continuous EEG recordings were segmented into epochs relative

to the TMS trigger, spanning -1000 ms to 1000 ms, with baseline correction applied from -500 ms to -20 ms. To mitigate decay-related artifacts, an exponential fitting method was employed. Additionally, the high-amplitude TMS artifact was addressed by excluding data within -2 ms to 10 ms around each TMS pulse, followed by cubic interpolation. Subsequently, visual inspection was performed to identify and reject epochs containing excessive artifacts and channels exhibiting persistent noise across most trials. The data were then downsampled from 5 kHz to 1 kHz before undergoing ICA, which was used to remove ocular and stereotypical artifacts based on the evaluation of independent components. Further artifact reduction was performed using TESA (The TMS-EEG Signal Analyser), an open-source extension for EEGLAB designed for TMS-EEG data processing. Within TESA, the SOUND algorithm applied spatial filtering to eliminate electrode polarization, line noise, and movement artifacts, while Signal-Space Projection with Source-Informed Reconstruction (SSP–SIR) was utilized to suppress muscle and sensory input artifacts, ensuring improved signal quality.(Mutanen et al., 2020, Rogasch et al., 2017) Finally, a zero-phase Butterworth band-pass filter (1–100 Hz) and a notch filter (48–52 Hz) were applied, and the data were subsequently re-referenced to the average reference.

### 2.10.3 Power spectral density (PSD)

The power spectral density of the preprocessed EEG data was computed using the pwelch method at sensor level, which provides an improved estimate of the power distribution over frequency by reducing variance. The resulting PSD values were used to analyze the power distribution across different frequency bands, including delta (1–4 Hz), theta (4–8 Hz), alpha (8–13 Hz), beta (13–30 Hz), and gamma (30-40 Hz). Power spectrum curves of two groups were also calculated. To compare the PSD of resting-state EEG between the PSD and

non-PSD groups, a two-sample t test was conducted after verifying the normal distribution of all data, across frequency bands (delta, theta, alpha, beta, and gamma). The receiver operating characteristic (ROC) curve and area under the curve (AUC) of the PSD in each frequency band were further used to classify PSD and non-PSD.

### 2.10.4 TMS-evoked cortical responses

TMS-evoked potentials (TEPs) are potentials elicited by TMS that reflect the temporal and spatial integration of excitatory and inhibitory postsynaptic potentials of cortical pyramidal cells and interneurons. The source-reconstructed signals were mapped onto the Brainnetome Atlas, which comprises 246 regions of interest (ROIs) across both hemispheres.(Fan et al., 2016) The template 3D T1-weighted anatomical images were used to perform the source reconstruction. The MRI pre-processing and mesh extraction were performed based on the FieldTrip toolbox running in the MATLAB environment and FreeSurfer (Version 6) on a Linux system. Image segmentation was conducted using a semi-automated pipeline in FreeSurfer, to get brain (2500 vertices), skull (2000 vertices), and scalp (1000 vertices), and to reconstruct head models. The conductivities of all tissues including white matter were taken as isotropic, as high-quality diffusion MRI data was not available for the patients that could have been used for estimation of the conductivity anisotropy. Then, triangle cortical meshes were extracted, downsampled (15684 dipoles). The lead field matrix, calculated from electrode locations, mesh, and head model, served as the basis for cortical source reconstruction via linearly constrained minimum variance (LCMV) beamforming. Following TMS, the activity of each dipole within the ROIs was derived using the first principal component from principal component analysis (PCA). To ensure the precision of the navigation procedure and justify the ROI selection, we additionally evaluated the spatial

distribution of TMS-evoked response. Following source reconstruction, each dipole's response was first normalized via a z-transformation relative to the baseline period (−300 to −20 ms) and then averaged over the 21–100 ms interval after the TMS pulse.

### 2.10.5 Auditory evoked potentials (AEPs)

In our study, we did not employ the recommended noise masking procedures. Instead, we provided earplugs to acute stroke patients, as the majority were unable to tolerate white noise, which has also been reported as a potential risk factor for delirium. To address the potential confounding effect of auditory stimulation, we extracted auditory evoked potentials (AEPs) elicited by TMS clicks during data analysis. Specifically, we obtained the cortical AEP components—N1 (80–120 ms) and P2 (160–200 ms)—by averaging TMS-evoked EEG signals recorded from eight electrodes surrounding the FCz location (F1, Fz, F2, FC1, FC2, C1, Cz, and C2). This approach was also validated in a previous work. The N1 and P2 components and their topographies are presented. Group comparisons of N1 and P2 amplitudes are also displayed, which were statistically assessed using two-sample t-tests between PSD and non-PSD group with a significance threshold of $p < 0.05$.

### 2.10.6 Fast perturbational complexity index ($PCI^{ST}$)

The $PCI^{ST}$ evaluates the cortex's capacity for complex causal interactions by measuring non-redundant state transitions across the principal components of evoked perturbation signals.(Comolatti et al., 2019) For each patient, $PCI^{ST}$ values were computed separately for stimulation of the bilateral DLPFC and SPL. Principal components were first chosen to account for at least 99% of the variance in response amplitude, with those exhibiting a signal-to-noise ratio

(SNR) ≤ 1.1 being excluded. Secondly, Matrices of amplitude distances comparing each time point of the signal with pre- and post-stimulus samples were calculated for each single component, separately. Thirdly, the distance matrices were applied a threshold at scale ε, producing the corresponding transition matrices. The mean number of state transitions during the response window (21–300 ms) was compared with that observed in the baseline period (−400 to −50 ms). Fourthly, we searched for the optimal scales by varying the threshold ε and comparing the average number of state transitions (NST) in the matrices of the post-stimulus (21 ms to 300 ms) with that of the pre-stimulus (-400 ms to -50 ms). The optimal scales were defined as at which the NST in the post-stimulus response were over and above the NST present in the pre-stimulus activity. Fifthly, the complexity of each component was defined as the maximized weighted difference of NST between post-stimulus response and pre-stimulus signals. Finally, $PCI^{ST}$ was calculated as the sum of these maximized significant state transitions across all principal components. The mean number of state transitions during the response window (21–300 ms) was compared with that observed in the baseline period (−400 to −50 ms).

### 2.10.7 Effective connectivity

We employed symbolic transfer entropy (STE) to evaluate effective connectivity, which is a variant of transfer entropy designed to characterize causal relationships between time-series data. For each EEG electrode, the recorded time-series were first transformed into symbol sequences representing the ordinal patterns of the data within each interval. STE was subsequently computed to quantify the directional information transfer triggered by TMS. Each electrode was assessed both as a sender and as a receiver. In particular, STE was computed for pairs of TEPs (21–400 ms) across electrodes using the recommended parameters: four symbols, a step interval of 16 ms, and a forward step of 50 ms.

### 2.10.8 Natural frequency

To examine TMS-induced oscillatory activity, event-related spectral perturbation (ERSP) analysis was conducted. The natural frequency is defined as the dominant frequency that intrinsically emerges with the highest power in a specific cortical region in response to evoked oscillations. Induced neuronal responses were extracted by removing each individual's mean response following the stimulus. Time–frequency representations (TFRs) were calculated for each ROI on a single-trial basis using a Hanning-tapered FFT with a frequency-dependent window of 3.5 cycles per time segment, 10 ms time steps, and 0.25 Hz frequency resolution across 4–45 Hz. EEG data spanning -1000 ms to 1000 ms around the TMS pulse ensured adequate time-frequency resolution. Single-trial normalization was performed via z-transformation and baseline correction by subtracting the average power from -300 ms to -20 ms. ERSPs were then extracted within -100 ms to 400 ms for statistical analysis. The natural frequency of each ROI was defined as the dominant frequency of TMS-evoked oscillations. To determine this, the power spectrum was calculated by averaging the oscillatory power from 21 to 400 ms of the ERSPs for each ROI, with the natural frequency corresponding to the peak in the resulting power spectrum.(Rosanova et al., 2009)

### 2.10.9 Lesion volume

First, DWI images were coregistered to each subject's T1-weighted images using Statistical Parametric Mapping (SPM12, https://www.fil.ion.ucl.ac.uk/spm/software/spm12/). Lesion maps were then manually outlined on the DWI images and independently verified by experienced clinicians using MRIcron (https://www.nitrc.org/projects/mricron).

The extent of the lesion was quantified by calculating the total number of affected voxels.

## 2.11 Statistical analysis

In this study, we employed several methods for statistical analysis. Continuous variables are reported as the mean ± standard deviation. Categorical variables are presented as frequencies with corresponding percentages. Group comparisons between PSD and non-PSD patients were performed using two-sample t-tests for normally distributed continuous variables (assessed with the Shapiro–Wilk test), Mann–Whitney U tests for non-normally distributed data, and Fisher's exact tests for categorical variables. A two-way repeated measures ANOVA was also used to examine the interaction between the stimulation targets and patient groups. Pearson correlation analysis was conducted to detect the correlation between TMS-EEG and clinical features as well as delirium duration. Significant cortical responses were identified using bootstrap sampling statistics. Brain excitability was quantified as the sum of the absolute values of these significant TEPs within 20–300 ms and compared between PSD and non-PSD groups using a two-sample t-test.

We used binary logistic regression to assess the performance of each single feature to predict delirium based on univariable model. Receiver operating characteristic curve (ROC) and area under ROC (AUC) were used to assess classification ability of each feature in predicting PSD. The cutoff value of the predictive model was calculated, which was defined when Youden index (specificity + sensitivity - 1) had the largest value. We also conducted paired comparison of areas under the ROC curves between ipsilesional SPL model and contralesional SPL model, as well as between ipsilesional DLPFC model and contralesional DLPFC model, to detect whether there was difference of predictive performance when stimulating bilateral hemisphere respectively.

After that, all these features were used to conduct the stepwise logistic regression (forward selected) to find the model with best fitting. The criteria of stepwise logistic regression were: 1) *p* value of each variable in the model < 0.05; 2) Akaike information criterion (AIC) is smallest. For the logistic regression model, the p-value and odds ratio (OR) with a 95% confidence interval (CI) were reported. Statistical significance was defined as a two-sided $p < 0.05$. To test the hypothesis that the TMS-EEG characteristics predict the delirium risk, while simultaneously assessing the interaction effect of the stroke lesion side on delirium risk, we additionally performed a two-way analysis of covariance (ANCOVA) for each TMS targets. SPSS 30.0 software package (IBM Corp., Armonk, New York, USA) and Prism 8 (Graph-Pad Software, CA, USA) were used for statistical analyses. We performed a subtraction analysis to determine whether lesion overlap differed between patients with PSD and non-PSD group. This subtraction analysis was conducted by subtracting the lesion overlap map of non-PSD patients from that of PSD patients.(Seifert et al., 2016) In addition, we conducted a voxel-based lesion–symptom mapping (VLSM) analysis to identify lesion sites associated with $PCI^{ST}$. Only voxels that were lesioned in at least two patients were included in the analysis. VLSM was performed using the NiiStat toolbox (https://github.com/neurolabusc/NiiStat) running in the MATLAB environment, and the results were displayed based on the ALLCAT atlas.(Catani and Thiebaut de Schotten, 2008, Tzourio-Mazoyer et al., 2002) Non-parametric permutation testing (2,000 permutations) was applied to correct for multiple comparisons.

# 3 Results

## 3.1 Patient characteristics

A total of 34 patients (20 males, 14 females) were included in the final analysis, of whom 13 (38%) developed PSD (PSD group), 21 other patients did not develop PSD (non-PSD group). Demographic characteristics (see also Table 1) did not differ significantly between groups (age: $p = 0.513$; gender: $p > 0.999$). The mean age was 79.38 and 77.52 years respectively, with a predominance of male participants in both groups (61.54% male in PSD group and 57.14% male in non-PSD group). Lesion laterality was comparable (predominantly left-sided; $p = 0.477$). However, lesion volume was significantly greater in the PSD group than in the non-PSD group (45.74 ± 42.74 vs. 8.44 ± 12.02 $cm^3$, $p = 0.001$). Similarly, NIHSS scores at the time of TMS-EEG assessment were higher in the PSD group (11.08 ± 8.57 vs. 4.52 ± 5.06, $p = 0.015$). The data were extracted from the digital patient records and discharge summaries of the University Hospital Tübingen. RMT did not differ between groups (68.85 ± 8.52% vs. 68.52 ± 8.95% of maximum stimulator output; $p = 0.917$), which was measured before TMS-EEG recording. The duration of delirium ranged from 1 to 14 days, the mean duration of which is 4.20, with a standard deviation of 3.23 and a median of 3.

**Table 1. Patient characteristics**

| | PSD group (n=13) | Non-PSD group (n=21) | p value |
|---|---|---|---|
| Age (years) | 79.38±7.47 | 77.52±8.67 | 0.513 |
| Gender (male), n (%) | 8 (61.54) | 12 (57.14) | >0.999 |
| Lesion side (right), n (%) | 4 (30.77) | 10 (37.04) | 0.477 |
| Lesion volume, $cm^3$ | 45.74±42.74 | 8.44±12.02 | **0.001*** |
| NIHSS score | 11.08±8.57 | 4.52±5.06 | **0.015*** |
| RMT (%MSO) | 68.85±8.52 | 68.52±8.95 | 0.917 |

Categorical variables were recorded as n (%), and continuous variables as means ± SD.
NIHSS = National Institutes of Health Stroke Scale; RMT = resting motor threshold; MSO = maximum stimulator output, PSD = post-stroke delirium.

## 3.2 Resting-state EEG spectral power

The averaged power spectrum curves across all electrodes for both groups were presented in Figure 1, demonstrating elevated low-frequency power in the PSD group. The differences in power spectral density between the two groups were analyzed across predefined frequency bands: delta (1–4 Hz), theta (4–8 Hz), alpha (8–13 Hz), beta (13–30 Hz), and gamma (30–40 Hz), using a two-sample t-test. The results revealed a significantly higher theta power in the PSD group ($p = 0.017$), whereas no significant differences were observed in the delta, alpha, beta, or gamma frequency bands. In the ROC curves, the power spectral density in the theta band (AUC = 0.749) demonstrated similar classification accuracy for PSD compared to clinical features such as NIHSS score and lesion volume.

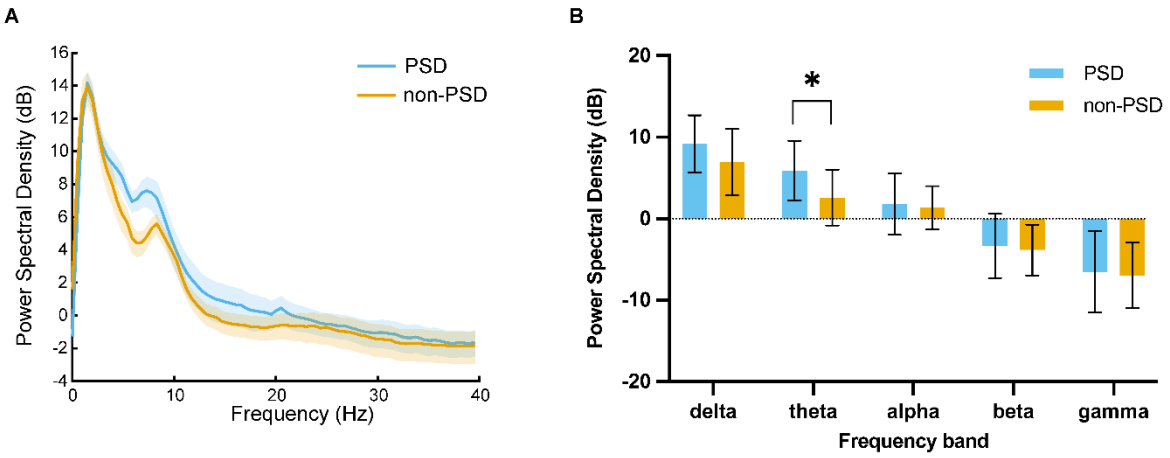


**Figure 1. Comparison of power spectral density of resting-state EEG between the two groups. A.** Averaged power spectrum curve of the PSD group (blue) and the non-PSD group (yellow) within the frequency range of 0-40 Hz over all electrodes at group level based on resting-state EEG, along with their respective 95% confidence intervals (shaded areas). **B.** Comparison of power spectral density (means ± 1SD) at defined frequency bands: delta (1–4 Hz), theta (4–8 Hz), alpha (8–13 Hz), beta (13–30 Hz), and gamma (30-40 Hz) between the PSD group (yellow) and the non-PSD group (blue). Horizontal dashed line represents 0 dB. * indicates a significant difference ($p < 0.05$).

## 3.3 TMS-evoked cortical responses

The TMS-evoked cortical responses were predominantly observed at the stimulation targets (red dots indicate neuronavigated bilateral DLPFC and SPL targets), the regions of interest (ROIs) defined by the Brainnetome Atlas (dark blue areas), and their surrounding areas (Figure 2). This finding confirms that the intended cortical targets were successfully activated by TMS. Source-reconstructed cortical potentials (TEP) at each stimulation site are displayed for both PSD and non-PSD groups. The TEP amplitudes of the two groups did not show very significant visual differences. We used two-sample t-tests to analyze differences in response intensity at each voxel between the two groups. Although no regions survived after multiple-comparison correction, the spatial distribution t-value maps of TMS-evoked response intensity revealed a widespread reduction in the PSD group compared to the non-PSD group, involving not only local activation regions but also cortical areas distant from the stimulation sites.

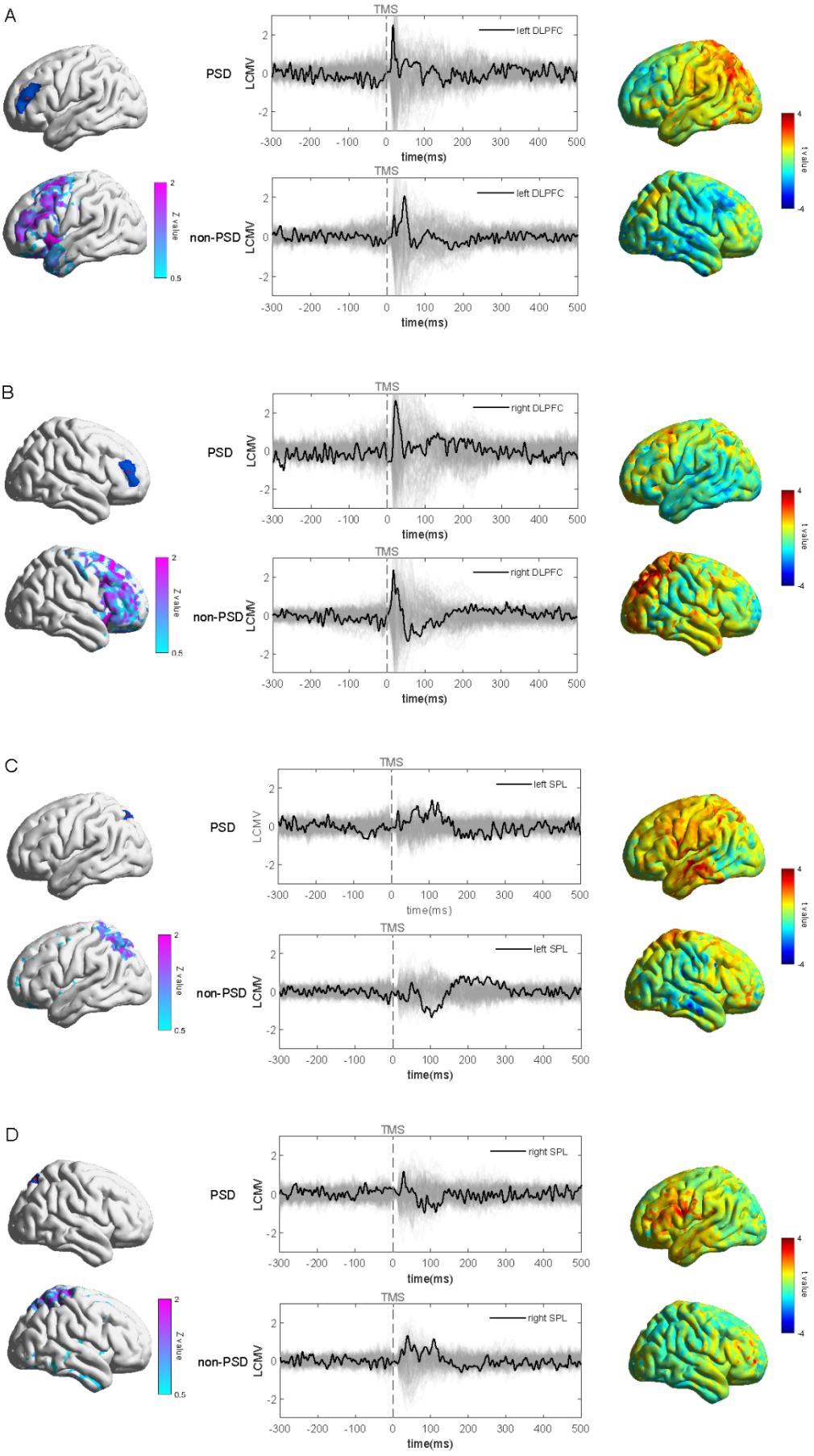
A
TMS
left DLPFC
PSD
LCMV
time(ms)
non-PSD
Z value
t value
B
right DLPFC
C
left SPL
D
right SPL

**Figure 2. Cortical responses evoked by transcranial magnetic stimulation (TMS). A-D.** The cortical surface map in the upper left panel illustrates TMS target regions of left DLPFC (A), right DLPFC (B), left SPL (C), and right SPL (D) in the Brainnetome Atlas (dark blue). The navigated TMS target sites are marked in red. The cortical surface map in the lower left panel depicts the spatial distribution of the average cortical response across all patients, where response size is defined as the absolute z-transformation relative to the baseline (−300 ms to −50 ms), elicited within 21-100 ms following the TMS pulse. The butterfly plot on the right displays the TMS-evoked cortical activity (y-axis: linearly constrained minimum variance [LCMV] values) averaged across all patients in the 246 regions based on the Brainnetome Atlas. The black traces represent the TMS-evoked responses in the target regions, while each gray trace corresponds to the TMS-evoked response from one other region. The cortical surface map in the right panel shows t value of two-sample t test between post-stroke delirium (PSD) and non-PSD groups. t value > 0 indicates higher values in the non-PSD group.

## 3.4 TMS-evoked cortical complexity ($PCI^{ST}$)

Across all stimulation targets, $PCI^{ST}$ was markedly lower in the PSD group compared to the non-PSD group (ipsilesional DLPFC: $p < 0.001$; contralesional DLPFC: $p < 0.001$; ipsilesional SPL: $p < 0.0001$; contralesional SPL: $p < 0.0001$; Figure 3). A two-way ANOVA revealed a main effect of group ($p < 0.0001$) but no significant interaction between stimulation site and group ($F(3,128) = 2.351$, $p = 0.075$), indicating a global reduction in perturbational complexity in the PSD group, prior to development of delirium. $PCI^{ST}$ values across all four stimulation sites showed significant inverse correlations with both lesion volume and NIHSS score (Figure 4, Figure 5), but no correlation with delirium duration. Regression lines and Pearson correlations with correlation coefficients (r) and *p* values are displayed in the figures.

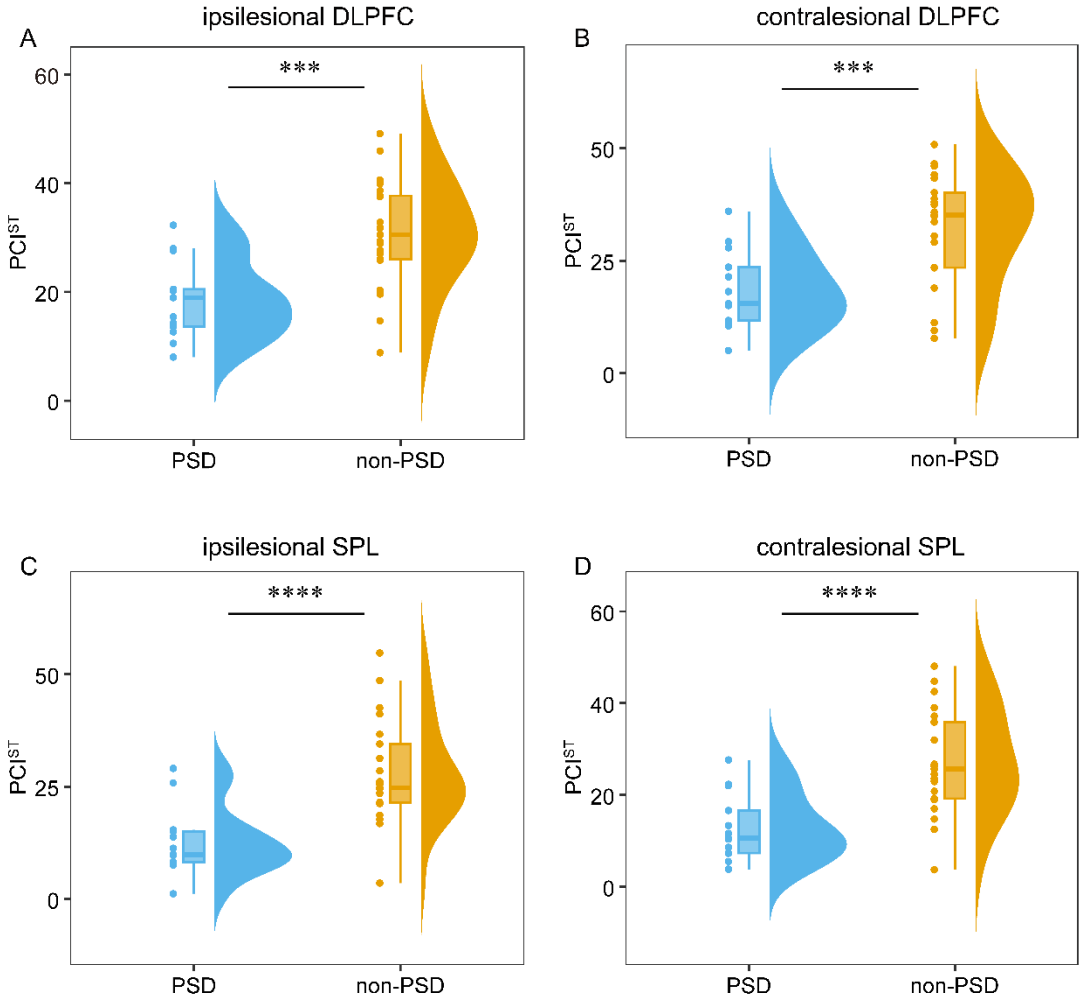


**Figure 3. Comparison of the fast perturbational complexity index ($PCI^{ST}$) between the two groups. A-D.** Half violin plot with scatter points of $PCI^{ST}$ when stimulating (**A**) ipsilesional dorsolateral prefrontal cortex (DLPFC), (**B**) contralesional DLPFC, (**C**) ipsilesional superior parietal lobule (SPL), (**D**) contralesional SPL, respectively, in the PSD group (blue) and the non-PSD group (yellow). Each dot corresponds one patient. Box and whisker plot shows median, quartiles, upper and lower whiskers (represent data within 1.5 × IQR from the quartiles). *** ($p<0.001$), **** ($p<0.0001$) indicate significant difference.

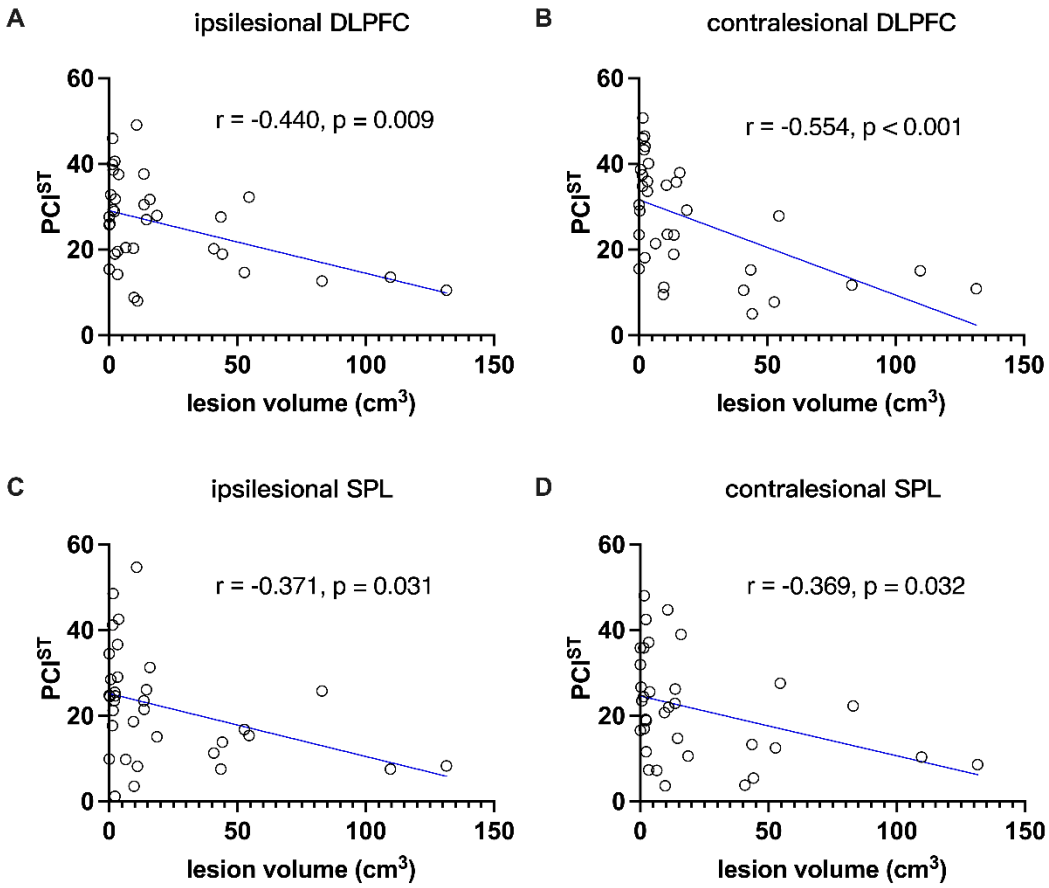


**Figure 4. Correlation of the averaged fast perturbational complexity index ($PCI^{ST}$) with stroke lesion volume.** The correlation of stroke lesion volume and $PCI^{ST}$ across four targets: ipsilesional dorsolateral prefrontal cortex (DLPFC) (A), contralesional DLPFC (B), ipsilesional superior parietal lobule (SPL) (C) and contralesional SPL (D). Regression lines and Pearson correlations with correlation coefficients (r) and p values are indicated. Each circle corresponds one patient of post-stroke delirium (PSD) group (red) and non-PSD group (black).

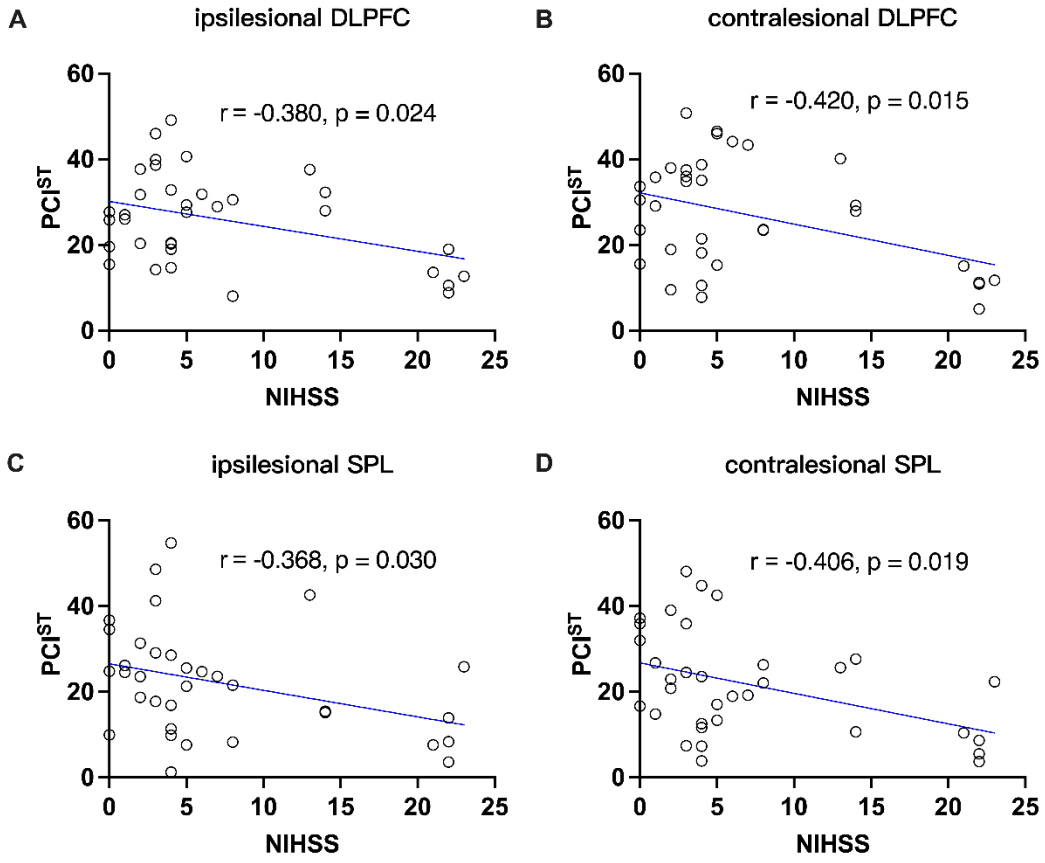


**Figure 5. Correlation of the averaged fast perturbational complexity index ($PCI^{ST}$) with clinical stroke severity. A.** The correlation of National Institutes of Health Stroke Scale (NIHSS) score at the time of measurement and averaged $PCI^{ST}$ across four targets: ipsilesional dorsolateral prefrontal cortex (DLPFC) (A), contralesional DLPFC (B), ipsilesional superior parietal lobule (SPL) (C) and contralesional SPL (D). Regression lines and Pearson correlations with correlation coefficients (r) and p values are indicated. Each circle corresponds one patient of post-stroke delirium (PSD) group (red) and non-PSD group (black).

## 3.5 Effective connectivity

We used STE to assess bidirectional information flow between each pair of electrode regions, with STE values representing the strength of effective connectivity. For each participant, an individual STE matrix was obtained, and

group differences were analyzed using two-sample t-tests. The t-value matrices representing differences between the PSD and non-PSD groups were visualized as heatmaps, showing that effective connectivity across multiple electrode regions was reduced in the PSD group. Furthermore, when electrodes were separately considered as senders and receivers, the t-values of STE were plotted as scalp topographies, revealing widespread reductions in effective connectivity in the PSD group regardless of whether the electrodes acted as senders or receivers. (Figure 6)

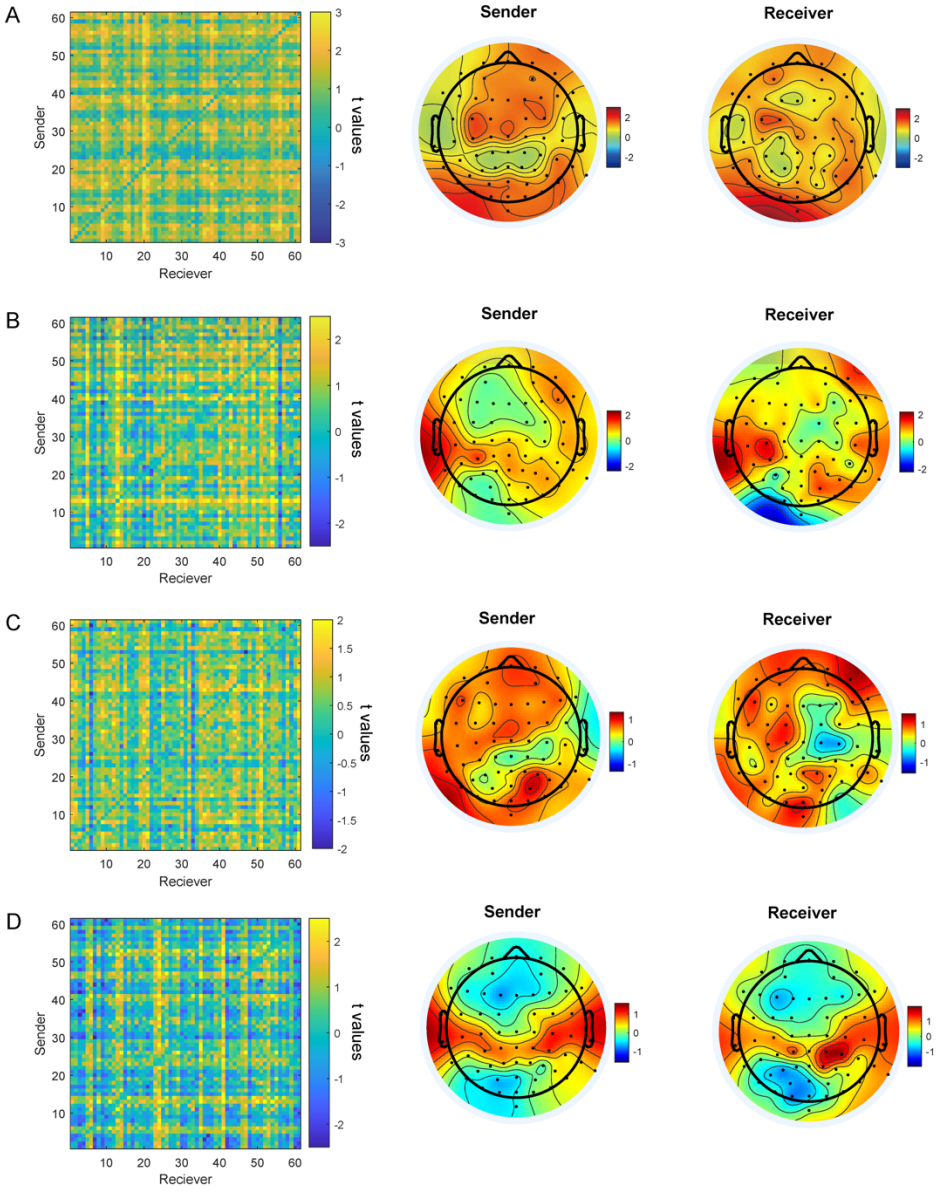

**Figure 6. Transcranial magnetic stimulation (TMS) evoked effective connectivity. A–D.** Left column shows t values matrix of symbolic transfer entropy (STE) based on two-sample t test between post-stroke delirium (PSD) and non-PSD group, with TMS targeting ipsilesional dorsolateral prefrontal cortex (DLPFC) (A), contralesional DLPFC (B), ipsilesional superior parietal lobule (SPL) (C) and contralesional SPL (D). Both the x-axis and y-axis represent electrode indices. Scalp topography shows t value distribution in whole brain regions when sending (middle) or receiving (right) information. t value > 0 indicates higher values in the non-PSD group.

## 3.6 Natural frequency

Natural frequency was significantly lower in the PSD group during stimulation of the ipsilesional DLPFC ($p$ = 0.014; Figure 7), but not at the contralesional DLPFC or bilateral SPL sites (all $p > 0.1$). No significant correlations were found between natural frequency and NIHSS, lesion volume, or duration of delirium at any site. In the ROC curves, the natural frequency when stimulating ipsilesional DLPFC (AUC = 0.718) showed lower accuracy for PSD compared to clinical features such as NIHSS score and lesion volume, as well as the power spectral density in the theta band.

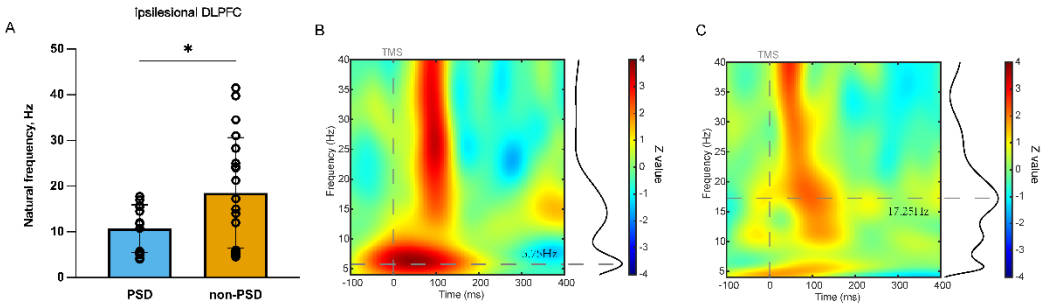


**Figure 7. Event-Related Spectral Perturbation (ERSP) and natural frequency. A.** Comparison of natural frequency (means ± 1SD) when stimulating ipsilesional dorsolateral prefrontal cortex (DLPFC) in the PSD-group (blue) and non-PSD group (yellow). Each circle corresponds to one patient. **B-C.** The time–frequency plots show the TMS-related ERSP extracted when stimulating ipsilesional DLPFC from (**B**) one representative patient of the PSD group and (**C**) one patient of the non-PSD group. The black curve at the right side of time-frequency plot depicts the power spectrum profile. The horizontal dashed lines indicate the corresponding natural frequency, i.e., the frequency of maximum power. * indicates a significant difference ($p < 0.05$).

## 3.7 Stroke lesions

Subtraction analysis of lesion overlaps between the two groups revealed that 83.11% of the lesion voxels associated with the occurrence of PSD were located in the white matter, involving the bilateral corona radiata, periventricular white matter, and basal ganglia regions. In addition, VLSM analysis demonstrated that lesions in the pyramidal tract were significantly associated with reduced averaged $PCI^{ST}$ across the four stimulation targets. (Figure 8)

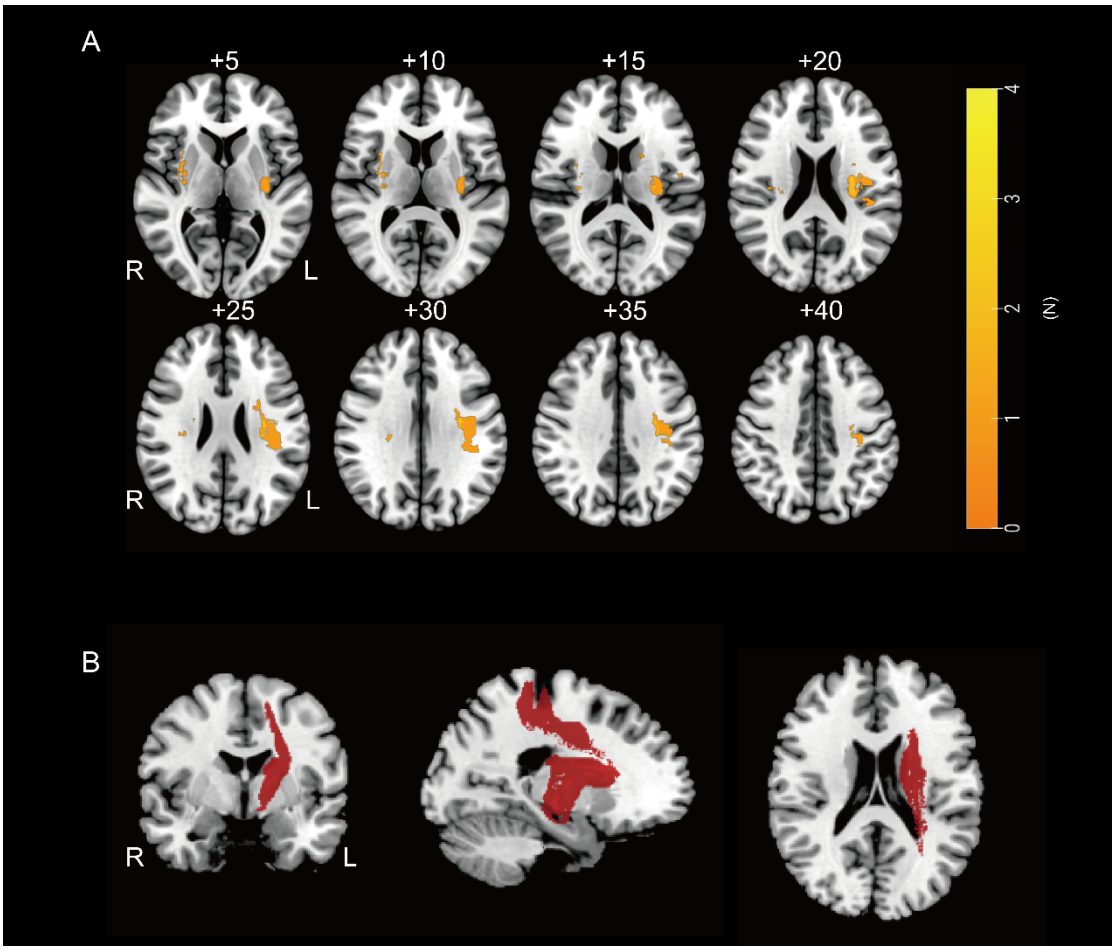


**Figure 8. Lesion overlap subtraction and voxel-based lesion–symptom mapping (VLSM) analysis. A.** After subtracting the lesion overlap of non-PSD patients from that of PSD patients, lesions in the bilateral corona radiata, periventricular white matter, and basal ganglia regions were found to be associated with PSD. Slice label based on MNI coordinate is displayed above images. **B.** Voxel-based lesion–symptom mapping (VLSM) analysis revealed that lesions in the pyramidal tract were significantly associated with a reduction in the averaged $PCI^{ST}$ value across the four stimulation sites: ipsilesional dorsolateral prefrontal cortex (DLPFC), contralesional DLPFC, ipsilesional superior parietal lobule (SPL) and contralesional SPL. L = left hemisphere; N = patient number of lesion overlaps after subtraction; R = right hemisphere.

## 3.8 Predictive performance of neurophysiological markers

We incorporated clinical variables (lesion volume and NIHSS score), resting-state EEG feature (theta band power), and TMS-EEG characteristics ($PCI^{ST}$ from stimulation of the four ROIs and natural frequency from ipsilesional DLPFC stimulation), which showed significant between-group differences, into univariable logistic regression models respectively. The results demonstrated that $PCI^{ST}$ provided superior predictive power for PSD compared to models incorporating lesion volume (AUC = 0.773), NIHSS score (AUC = 0.747), theta band power (AUC = 0.749), or natural frequency (AUC = 0.718). Among the models including $PCI^{ST}$, the best predictive performance was observed when stimulating the ipsilesional SPL (AUC = 0.874). The AUC with target of ipsilesional DLPFC, contralestional and contralesional SPL are 0.816, 0.814 and 0.845. Stepwise multivariable logistic regression did not identify any model outperforming the univariate $PCI^{ST}$ (ipsilesional SPL) model. When $PCI^{ST}$ (ipsilesional SPL) was entered into a multivariable model alongside NIHSS and lesion volume, only $PCI^{ST}$ remained a significant independent predictor ($p$ = 0.018 vs. $p$ = 0.585 and $p$ = 0.078; Table 2a). The same held true for $PCI^{ST}$ from contralesional SPL ($p$ = 0.034 vs. $p$ = 0.679 and $p$ = 0.078; Table 2b), underscoring the robustness of $PCI^{ST}$ as a predictor of PSD independent of clinical and structural lesion severity. Optimal $PCI^{ST}$ thresholds for PSD classification were 16.1 (ipsilesional SPL) and 16.8 (contralesional SPL), based on Youden's index.

**Table 2. Multivariate logistic regression involving $PCI^{ST}$_ipsilesional SPL and clinical and neuroimaging features**

| | P value | B value | Standard error | OR | OR 95% CI | | AIC of model |
|---|---|---|---|---|---|---|---|
| | | | | | lower | upper | |
| $PCI^{ST}$_ipsilesional SPL | **0.018*** | -0.170 | 0.072 | 0.844 | 0.711 | 0.949 | 30.85 |
| NIHSS | 0.585 | -0.053 | 0.096 | 0.949 | 0.774 | 1.160 | |
| Lesion volume | 0.078 | 0.055 | 0.031 | 1.057 | 1.001 | 1.139 | |

**Table 3. Multivariate logistic regression involving $PCI^{ST}$_contralesional SPL and clinical and neuroimaging features**

| | P value | B value | Standard error | OR | OR 95% CI | | AIC of model |
|---|---|---|---|---|---|---|---|
| | | | | | lower | upper | |
| $PCI^{ST}$_contralesional SPL | **0.034*** | -0.136 | 0.064 | 0.873 | 0.751 | 0.971 | 33.54 |
| NIHSS | 0.679 | -0.039 | 0.094 | 0.962 | 0.789 | 1.175 | |
| Lesion volume | 0.078 | 0.052 | 0.029 | 1.053 | 1.002 | 1.129 | |

$PCI^{ST}$ = fast perturbational complexity index; NIHSS = National Institutes of Health Stroke Scale; AIC = Akaike information criterion.

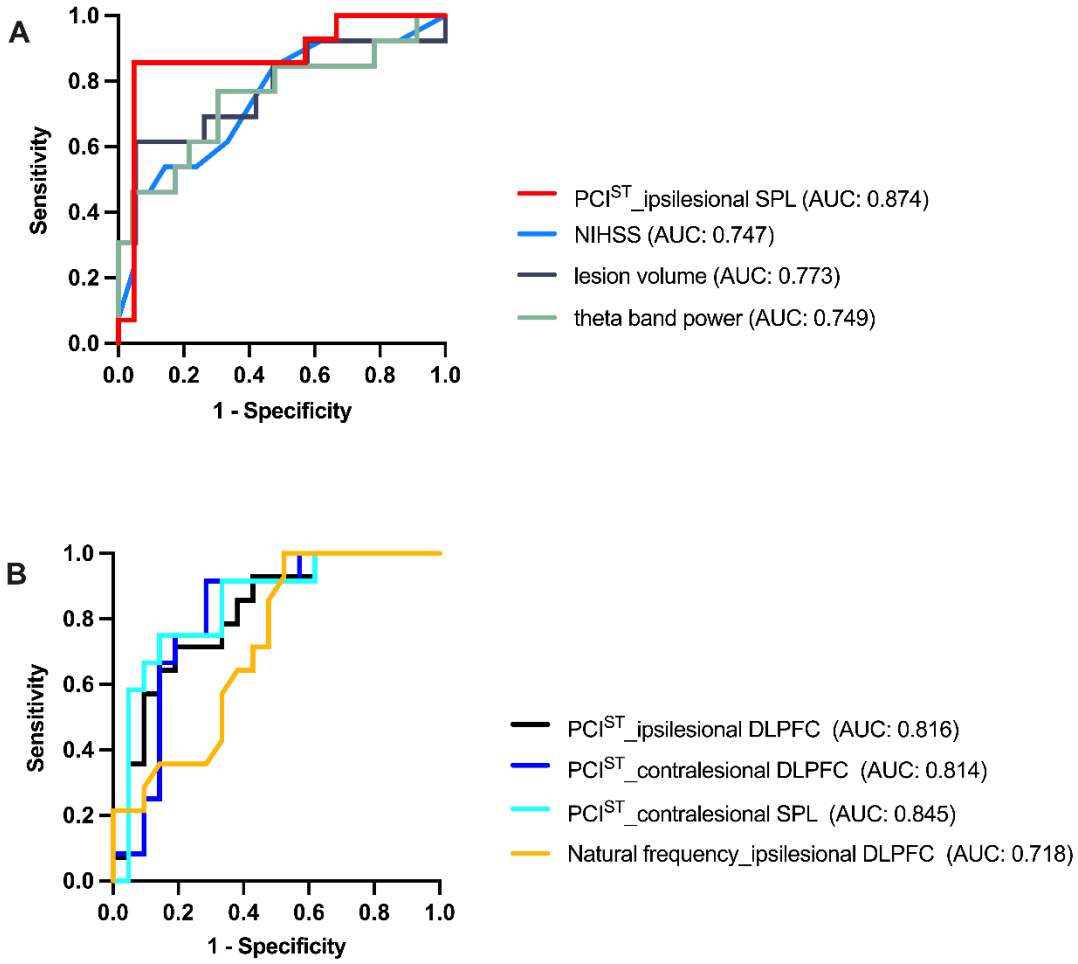


**Figure 9. Receiver operating characteristic curves (ROC) for classification of PSD vs. non-PSD. A.** ROC of the univariate model involving fast perturbational complexity index ($PCI^{ST}$) when stimulating ipsilesional superior parietal lobule (SPL), National Institutes of Health Stroke Scale (NIHSS) score at the time of measurement, stroke lesion volume and resting-state EEG theta band power, respectively. **B.** ROC of the univariate model involving $PCI^{ST}$ when stimulating ipsilesional dorsolateral prefrontal cortex (DLPFC), contralesional DLPFC, contralesional SPL and natural frequency when stimulating ipsilesional DLPFC, respectively. Area under the curve (AUC) is indicated.

### 3.9 Interaction effect of stroke lesion side on delirium risk prediction with perturbational complexity index ($PCI^{ST}$)

To test the hypothesis that the TMS-EEG characteristics predict the delirium risk, while simultaneously assessing the interaction effect of the stroke lesion side on delirium risk, we additionally performed a two-way analysis of covariance (ANCOVA) for each TMS targets. We found no evidence (Figure 10) for interaction effect of stroke lesion side in predicting delirium with $PCI^{ST}$, the results of which is F (1, 30) = 0.091，$p$=0.765 for ipsilesional DLPFC; F (1, 30) = 0.102，$p$=0.752 for contralesional DLPFC; F (1, 30) = 0.069，$p$=0.795 for ipsilesional SPL; F (1, 30) = 0.379，$p$=0.543 for contralesional SPL.

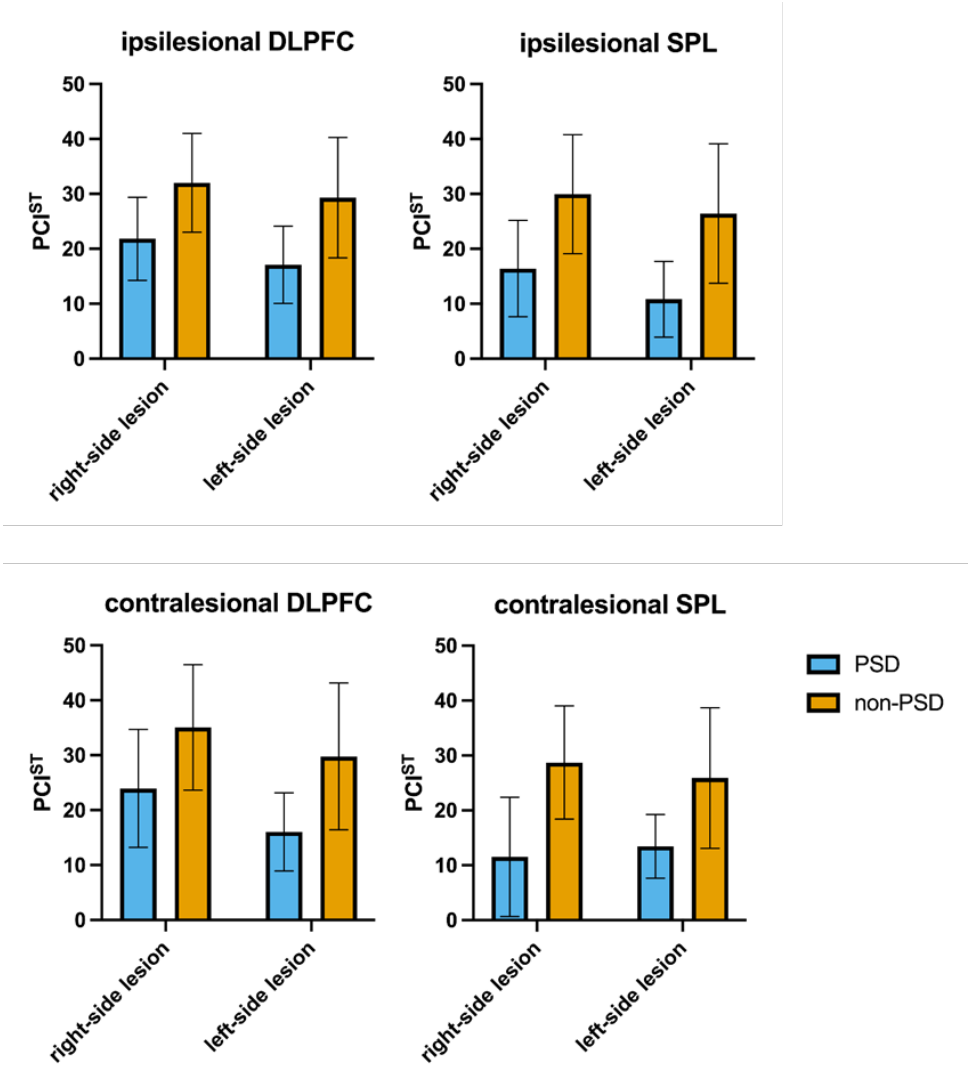

**Figure 10. Interaction effect of stroke lesion side on delirium risk prediction with perturbational complexity index ($PCI^{ST}$).** Perturbational complexity index ($PCI^{ST}$) obtained with transcranial magnetic stimulation (TMS) targeting four regions of interest (ROI) of bilateral brain in patients of the post-stroke delirium (PSD) vs. non-PSD group and right-side lesion vs. left-side lesion group. Bars and error bars show mean $\pm$ 1SD of $PCI^{ST}$. Blue color represents PSD patients; yellow color non-PSD patients.

## 3.10 Auditory evoked potentials (AEPs)

We obtained the cortical AEP components—N1 (80–120 ms) and P2 (160–200 ms)—by averaging TMS-evoked EEG signals recorded from eight electrodes surrounding the FCz location (F1, Fz, F2, FC1, FC2, C1, Cz, and C2). The N1 and P2 components and their topographies are presented in Figure 11. Group comparisons of N1 and P2 amplitudes are also displayed in Figure 12 and no significant difference were found between PSD and non-PSD group in any of the fours TMS targets, which were statistically assessed using two-sample t-tests with a significance threshold of $p < 0.05$.

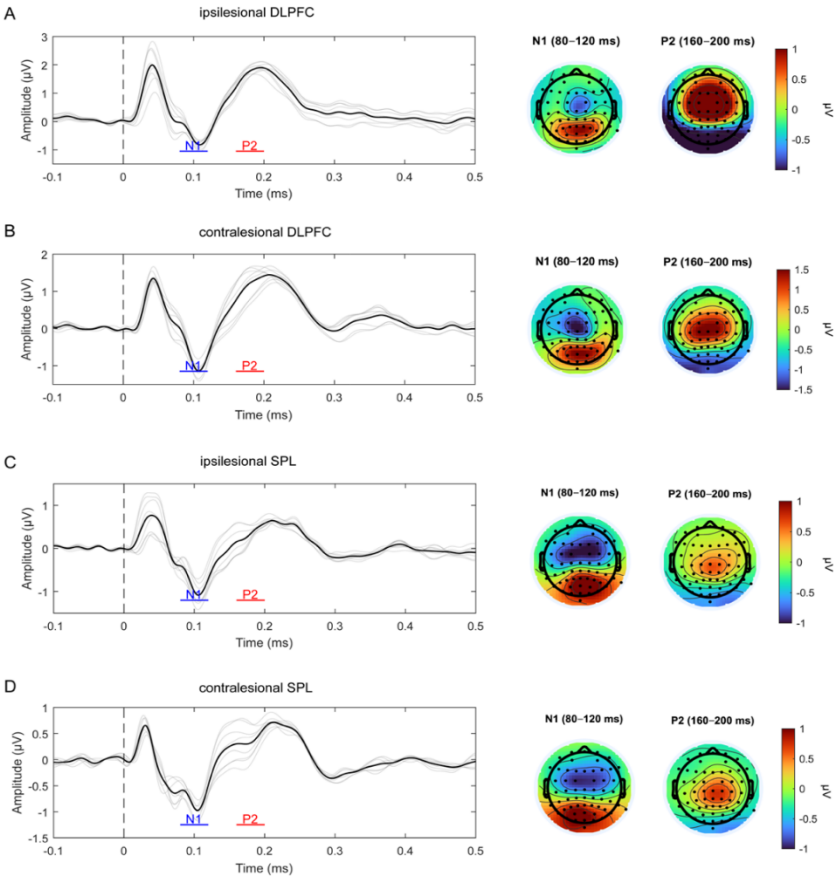


**Figure 11. Auditory evoked potentials (AEPs).** The figures show transcranial magnetic stimulation (TMS)-evoked EEG potentials (TEPs) averaged across all patients (n=34), recorded over eight electrodes surrounding FCz (F1, Fz, F2, FC1, FC2, C1, Cz and C2) when stimulating **(A)** ipsilesional dorsolateral prefrontal cortex (DLPFC), **(B)** contralesional DLPFC, **(C)** ipsilesional superior parietal lobule (SPL), and **(D)** contralesional SPL. In the butterfly plots, each gray line represents signal from one electrode, with the black line showing the grand average. Blue and red horizontal bars underneath the TEP recordings display the defined time windows of the N1 (80-120 ms) and P2 (160-200 ms) AEP components evoked by the TMS clicks. Right panels show the N1 and P2 topographies, with color coding amplitude (μV).

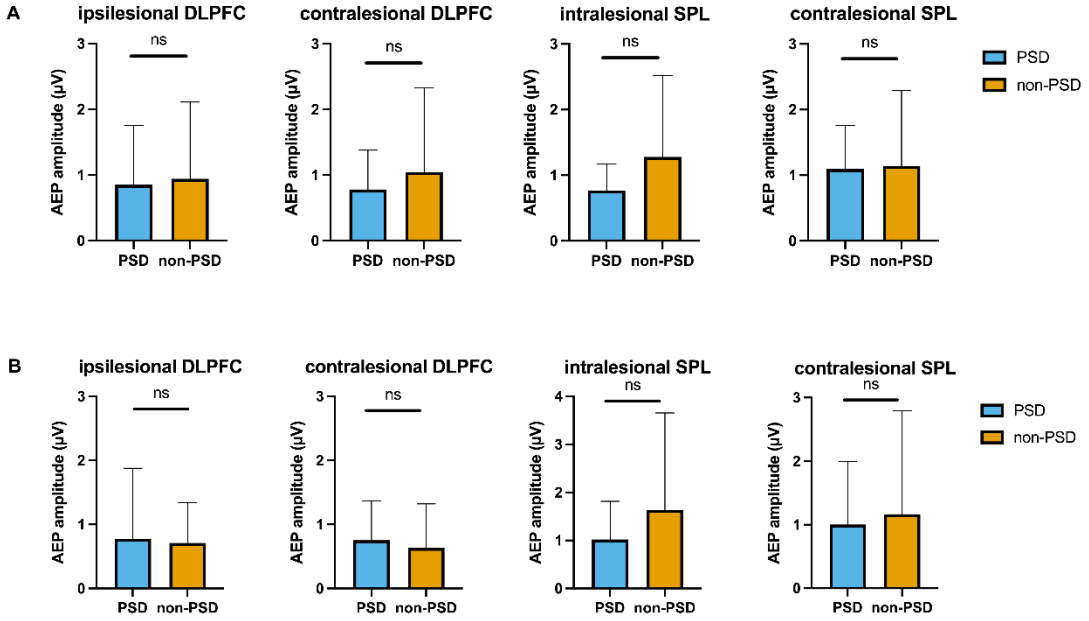


**Figure 12. Auditory evoked potentials (AEPs) in post-stroke delirium (PSD) and non-PSD patients.** AEPs amplitude is given by averaging absolute values in eight channels surrounding FCz (F1, Fz, F2, FC1, FC2, C1, Cz and C2). Amplitudes for **(A)** N1 and **(B)** P2 were averaged in time windows of 80-120 ms and 160-200 ms, respectively. Bars and error bars show means $\pm$ 1SD of the N1 and P2 AEP components in the non-PSD vs. PSD groups. Note that AEPs showed no significant difference between groups.

# 4 Discussion

In this prospective study of stroke patients we employed TMS–EEG to investigate cortical reactivity, excitability, and effective connectivity, particularly perturbational complexity, and to evaluate the predictive power of these measures for PSD. Our findings demonstrate that $PCI^{ST}$ offers robust and independent predictive value for the subsequent development of PSD—outperforming established clinical markers such as NIHSS and lesion volume, as well as resting-state EEG features. Notably, the predictive accuracy of $PCI^{ST}$ was consistent across the ipsilesional and contralesional hemispheres and the DLPFC and SPL stimulation sites, without interaction effect of lesion side, underscoring its potential as a generalizable and mechanistically informative biomarker. These results hold translational relevance, as they may enable early risk stratification and the development of targeted preventive strategies in the stroke unit or ICU setting. Previous studies on predicting PSD have often focused on clinical indicators. However, single or combined clinical risk factors cannot reliably predict delirium. Although they are correlated with its occurrence, they provide little mechanistic explanation for delirium, which contributes to their limited predictive power. In contrast, we found that $PCI^{ST}$ not only demonstrated strong predictive performance but also offered a mechanistic explanation for PSD from the perspective of brain network dynamics.

## 4.1 Demographics and clinical features

Among the 34 patients included in our analysis, 38% developed delirium, exceeding the 25% incidence typically reported in unselected stroke populations.(Shaw et al., 2019) This elevated rate likely reflects the advanced age of our cohort (mean 78.23 years), which is consistent with prior meta-analytic data showing a PSD prevalence of 34% among patients aged 75–79 years.(Ye et al., 2024) While some studies have implicated right-hemispheric

strokes as a specific risk factor for PSD,(Oldenbeuving et al., 2011) others have found no such association(Rhee et al., 2022); our study similarly did not find lateralization effect. In addition, previous studies have not provided a reasonable and convincing explanation for the increased risk of delirium following right-hemispheric stroke. I believe this scientific question needs to be validated with larger-sample data in the future, and if specific effects are detected, the underlying mechanisms should be further explored and explained. In contrast, both lesion volume and NIHSS score were significantly higher in the PSD group, in line with previous work identifying stroke severity as a key risk factor for delirium.(Alvarez-Perez and Paiva, 2017) Severe strokes are often accompanied by extensive brain tissue damage, affecting regions involved in attention, cognition, and arousal. Large-scale brain lesions can disrupt the integration and transmission of neural networks, impairing the functional integrity of cortico-cortical and cortico-thalamo-cortical circuits, thereby increasing the risk of delirium. Patients with severe strokes frequently have pre-existing cognitive impairment, which reduces their “buffering capacity” against further brain dysfunction and makes them more susceptible to acute cognitive disturbances. In addition, these patients often require ICU or critical care, sedation, or mechanical ventilation, all of which further increase the risk of delirium. However, our predictive model results indicate that the sensitivity and specificity of NIHSS and lesion volume are not sufficiently high, possibly because neither of these measures specifically reflects the impairment of critical functions, such as cognition or attention, or damage to a particular brain network, and therefore cannot accurately identify the risk of delirium.

## 4.2 Resting-state EEG

During delirium, the resting-state EEG is characterized by a predominance of slow oscillations and a reduction in fast oscillations, with these changes most

significant in the frontal and parietal regions. However, to investigate the mechanisms underlying delirium and identify its risk, it is necessary to assess quantitative EEG features prior to the onset of PSD. Analysis of resting-state EEG in our study revealed elevated theta-band power in patients who later developed delirium. This finding aligns with prior prospective data linking relative theta power to delirium risk.(Williams Roberson et al., 2023) Another study assessed the median dominant frequency (MDF) from the prefrontal regions—a resting-state EEG biomarker based on intrinsic alpha oscillations that indicate a baseline cortical state. The results showed that reduced preoperative MDF was associated with postoperative delirium, and a lower MDF also indicates that cortical oscillatory activity at that time was shifted closer to the theta frequency range.(Kim et al., 2023) Under normal conditions, theta oscillations are closely associated with the regulation of attention, working memory, learning, and synchronization within hippocampal–cortical circuits. In the brains of children and adolescents, theta activity is relatively strong and contributes to cognitive development; however, in adults, only mild theta activity is commonly observed during focused attention or introspective states.(Herweg et al., 2020, Cellier et al., 2021) Excessive or abnormally enhanced theta oscillations are often linked to brain dysfunction, such as cognitive impairment, delirium, dementia, and post-stroke cortical abnormalities. In particular, during delirium and other acute brain dysfunctions, EEG typically shows increased low-frequency theta activity and decreased high-frequency beta/alpha activity, reflecting desynchronization of thalamo-cortical networks and impaired cognitive control. Theta activity in the awake adult brain is generally interpreted as a marker of cortical dysfunction, potentially reflecting metabolic stress, hypoxia, or neuroinflammatory processes.(Faigle et al., 2013, Ingvar et al., 1976) Moreover, theta oscillations are critically involved in the functional architecture of top-down attention.(Fleischmann et al., 2019) Aberrant increases in theta power may disrupt attention, impulse control, and working memory—core domains often impaired during delirium.(Angelidis et al., 2016,

Helfrich et al., 2018) These changes likely arise from both structural disconnection following stroke and secondary injury mechanisms, including oxidative stress and inflammatory activation.(Maldonado, 2018, Smith et al., 2024) Importantly, our EEG recordings were acquired prior to delirium onset, suggesting that elevated theta power may be an early pathophysiological signature rather than a consequence of delirium itself.(Jacobson and Jerrier, 2000) However, we did not observe differences in the power spectral density of other frequency bands between the PSD and non-PSD groups. Notably, the delta-band power was not significantly reduced in the PSD group. We interpret the reduction of delta power as an EEG abnormality that has not yet emerged prior to the onset of delirium, which represents a further deterioration of cortical function. In the predictive model, the AUC of theta-band power spectral density was comparable to that of NIHSS and stroke volume, and did not demonstrate superior predictive ability for delirium.

## 4.3 Natural frequency

Compared to passive observation of neural activity via EEG, TMS–EEG enables causal probing of cortical network responsiveness. The natural frequency—a region-specific measure of oscillatory reactivity to stimulation(Vallesi et al., 2021)—was lower in the PSD group compared to the non-PSD group only when stimulating the ipsilesional DLPFC. This pattern likely reflects localized disruption of cortico-subcortical connectivity, as the natural frequency typically declines when intrinsic resonance mechanisms are compromised.(Capilla et al., 2022) In TMS–EEG research, the natural frequency refers to the dominant oscillatory frequency at which a specific cortical region intrinsically resonates in response to external perturbation (TMS pulse). This frequency reflects the intrinsic properties of local cortical circuits, including the balance between excitatory and inhibitory synaptic activity, and

the connectivity of pyramidal neurons with interneurons.(Rosanova et al., 2009) Natural frequency can vary across brain regions, with slower frequencies in posterior regions and faster frequencies in anterior regions.(Vallesi et al., 2021) Assessing natural frequency via TMS–EEG provides insight into regional cortical excitability and functional state, and deviations from expected frequencies may indicate network dysfunction, cortical slowing, or impaired thalamo-cortical interactions. The DLPFC is a central hub of the frontoparietal control network (FPCN), which supports executive function and cognitive control. Its functional impairment has been consistently associated with the onset of delirium.(Cole et al., 2014) However, in the prediction model, the natural frequency of the ipsilesional DLPFC showed the poorest predictive ability for PSD, with an AUC lower than that of NIHSS and lesion volume, indicating that it cannot serve as a reliable predictor.

## 4.4 TMS-evoked cortical responses and effective connectivity

TMS-evoked cortical responses reflect cortical excitability, while effective connectivity reflects the ability of information to be transmitted within brain networks and the brain's capacity to integrate external stimuli. During delirium, the brain enters a state of disconnection, often characterized by reduced cortical excitability, lower response intensity, shorter response durations, and decreased effective connectivity between regions, resulting in impaired processing of external information. This underlies the attention deficits and cognitive impairments observed in patients with delirium. A theoretical framework has been proposed suggesting that the risk of delirium depends on acute changes in inhibitory synaptic signaling and reduced neural network connectivity. According to this hypothesis, the delirium syndrome arises from enhanced inhibitory tone leading to disintegration of neural networks.(Sanders, 2011) In addition to inhibitory neurotransmission, parallel increases in

cholinergic and aminergic signaling (e.g., norepinephrine or dopamine) may facilitate interaction with the environment even under a reduced level of consciousness, which is characteristic of delirium.(Hshieh et al., 2008) Similarly, connectivity may change differentially across brain regions, with increases in some areas and decreases in others, potentially contributing to the heterogeneous symptoms of delirium.

In our study, we computed cortical responses and effective connectivity in both groups. We observed that, in the PSD group, cortical responses and effective connectivity were reduced across widespread brain regions compared with the non-PSD group, although these differences did not reach statistical significance. This may be attributable to the advanced age of our patients, who generally exhibit lower baseline cortical responses and effective connectivity compared to younger populations. Moreover, prior to the onset of delirium, these reductions may not be as pronounced as during an active delirium episode, making it difficult to detect statistically significant differences between the PSD and non-PSD groups.

## 4.5 Fast perturbational complexity index

The most salient and consistent finding in our study was a universal reduction in $PCI^{ST}$ among patients who developed PSD, irrespective of stimulation site. $PCI^{ST}$ quantifies the spatiotemporal complexity of TMS-evoked cortical activity, reflecting the brain's capacity for integrated, differentiated processing.(Comolatti et al., 2019, Wang et al., 2022, Xu et al., 2024, Wang et al., 2023) Delirium is increasingly conceptualized as a disorder of several interacting brain networks, characterized by hypoconnectivity and aberrant antagonism. The FPCN, DAN, DMN, and salience network (SN) form a dynamic attentional control architecture.(Young, 2017, Menon and Uddin, 2010,

Sridharan et al., 2008) When inhibitory control from FPCN and SN over DMN is impaired, internally generated content such as hallucinations may become unconstrained.(Christoff et al., 2016, Gerrans, 2014, Coltheart, 2007) These disruptions are thought to be potentiated by stroke-related neurotransmitter imbalances—especially reduced cholinergic and excessive monoaminergic signaling.(da Costa Rodrigues et al., 2022, Bleck, 2018) $PCI^{ST}$ may capture this network fragility in a compact and actionable format.

In addition, reduced $PCI^{ST}$ in this context likely reflects a fundamental collapse in the brain's ability to sustain temporally precise, spatially distributed, and causally coherent patterns of cortical activity. This can be interpreted as a failure of re-entrant processing and thalamo-cortical synchronization, both of which are essential for conscious cognitive operations.(Brunia, 2001) In delirium, functional disconnection of these thalamo-cortical loops is thought to contribute to the breakdown of integrative capacity.(van Montfort et al., 2019, Boukrina et al., 2022, Sanders, 2011, van Dellen et al., 2014) $PCI^{ST}$, as a complexity-based measure of effective connectivity, is exquisitely sensitive to TMS perturbations. It reflects the capacity of large-scale networks to sustain reverberant signal propagation in response to external stimulation—a capacity that critically depends on thalamo-cortical and cortico-cortical integrity. Its reduction reflects a diminished capacity of large-scale neural networks to sustain reverberant signal propagation in response to external stimulation—largely attributable to impaired thalamo-cortical and cortico-cortical integrity. Our symbolic transfer entropy (STE)-based effective connectivity analysis corroborated this finding, showing a widespread decrease of STE in the PSD group across scalp electrodes when considered both as senders and receivers.

This interpretation is supported by prior TMS–EEG studies in disorders of consciousness and anesthesia, where reduced $PCI^{ST}$ has been linked to impaired thalamo-cortical dynamics.(Wang et al., 2022, Xu et al., 2024) Our lesion overlap subtraction showed that if the lesion involves the projection fibers

between the cortex and thalamus, delirium is more likely to occur. Further VLSM analysis found that lesions located on the pyramidal tract (PT) were significantly correlated with $PCI^{ST}$ values. Although PT lesions are traditionally considered to primarily affect motor function, emerging evidence suggests that PT damage can independently influence cognitive performance following stroke.(Puy et al., 2018) Moreover, associations between reduced fractional anisotropy of PT and the emergence of neupsychiatric symptoms have been reported.(Luttenbacher et al., 2022) This is because there are also many critical connections between the various parts of the complex cortico–thalamo–cortical loop.(Shepherd and Yamawaki, 2021, Gómez-Ocádiz and Silberberg, 2023) Future studies should further explore the relationship between damage of corticothalamic projection and reduced $PCI^{ST}$ based on more samples to provide a more detailed mapping atlas. Although the occurrence of delirium and the reduction of $PCI^{ST}$ are affected by these strategic lesions, $PCI^{ST}$ reductions reliably predict PSD across different stimulation sites, independent of lesion laterality—highlighting $PCI^{ST}$ as a reproducible and generalizable network biomarker.

Importantly, our results also demonstrate that $PCI^{ST}$ is not only a mechanistically meaningful marker, but also clinically feasible, robust, and reproducible under real-world conditions. Despite the logistical challenges inherent to neurophysiological measurements in the stroke unit or ICU, we successfully acquired high-quality TMS–EEG data in the acute phase after stroke in the majority of patients. $PCI^{ST}$ values proved promising to inform individual risk stratification, establishing the method’s reliability in stroke patients. This positions $PCI^{ST}$ as a candidate biomarker ready for clinical translation.

## 4.6 Indications for the future

Looking forward, the priority must be to streamline TMS–EEG acquisition and $PCI^{ST}$ analysis for routine bedside implementation. With improvements in automation, real-time signal processing, and user-friendly interfaces, TMS–EEG could become a practical point-of-care tool for delirium prediction. Although $PCI^{ST}$ was negatively correlated with both NIHSS score and lesion size, it was identified as an independent risk factor, suggesting that reduced brain complexity may serve as a common core pathway underlying the progression to delirium following stroke. This finding is of great significance for further exploring the pathophysiological mechanisms of PSD. As a global index, $PCI^{ST}$ reduction being independent of the stimulation side aligns with our expectations. Importantly, this provides greater flexibility in selecting the stimulation side for future clinical applications. Furthermore, if only a single target (for example either side SPL) needs to be stimulated for delirium risk prediction, the measurement time can be significantly reduced, enhancing patient comfort and tolerance. We also established a cutoff value for predicting PSD, which can serve as a reference for future studies.

Considering that current preventive interventions of delirium for specific acute stroke patient populations are still limited to general non-pharmacological treatments with inconclusive evidence—such as early mobilization, fluid/electrolyte balance, visual/hearing aids, sleep regulation, and pain management—our findings on impaired brain network connectivity and reduced complexity based on TMS-EEG suggest that neuromodulation using TMS may represent a promising preventive intervention for patients at risk of delirium. In patients with disorders of consciousness, studies have already provided evidence that applying 10Hz repetitive transcranial magnetic stimulation (rTMS) to the left DLPFC can significantly enhance consciousness levels in patients with a minimally conscious state.(Xu et al., 2024) Similarly, future research should explore the potential of rTMS in reducing delirium risk. This approach

could lead to the development of a TMS-EEG-based sequential delirium management strategy that integrates risk identification with preventive intervention, ultimately benefiting stroke patients.

## 4.7 Limitations

Several limitations merit discussion. First, although our findings were robust within the studied cohort, external validation in larger samples will be important. Second, we employed earplugs rather than noise masking during TMS delivery, due to evidence that auditory masking may increase delirium risk in stroke and reduce patient tolerance. However, we further analyzed the auditory evoked potentials (AEPs) and ruled out their potential as a confounding factor in our results. Third, for patients without individual MRIs, we used a standardized template for neuronavigation. While acceptable in this setting, future developments in portable, ICU-adapted navigation systems may further enhance precision and feasibility. Fourth, the operation of TMS-EEG remains relatively complex, the examination process is time-consuming, and it can be burdensome for acute stroke patients. Therefore, it is hoped that increased clinical interest in TMS-EEG will drive the development and simplification of this technology, enabling this important method to become more widely available in the near future. Finally, although the current TMS-EEG data processing workflow is relatively standardized, there are still some parameter differences and minor variations between pipelines. It is hoped that, in addressing specific scientific questions in the future, as consistent a processing procedure as possible will be used.

# 5 Summary

Delirium is a frequent and severe complication in the acute phase after stroke, yet reliable predictors of its occurrence are lacking. Emerging evidence implicates disturbed large-scale brain network dynamics as a key mechanism leading to delirium. Transcranial magnetic stimulation combined with electroencephalography (TMS-EEG) provides a promising approach to assess cortical network responsiveness and response complexity *in vivo*.

In this study we investigated to what extent the TMS-EEG features, especially fast perturbational complexity index ($PCI^{ST}$), a TMS-EEG measure of response integration and differentiation, predict the development of PSD when tested within the first 48 hours after stroke onset but prior to delirium onset.

We prospectively enrolled 34 acute stroke patients admitted to the stroke unit. In addition to resting-state EEG, TMS-EEG were recorded by targeting the dorsolateral prefrontal cortex (DLPFC) and superior parietal lobule (SPL) of the ipsilesional and contralesional hemisphere. Delirium was assessed every 8 hours using the Intensive Care Delirium Screening Checklist (ICDSC) and DSM-5 criteria. $PCI^{ST}$ and natural frequency were extracted from TMS-evoked EEG responses; resting-state EEG spectral power was also analyzed. Predictive performance was evaluated using logistic regression, ROC analysis, and correlations with clinical and imaging markers, including NIHSS and lesion volume.

In our study, thirteen patients (38%) developed delirium. Patients in PSD group had higher NIHSS score, larger lesion volume, and increased theta-band power in resting-state EEG, compared with the non-PSD group. However, these measures showed limited predictive ability for PSD. In TMS-EEG–based analyses, although we observed a decrease in the natural frequency of the ipsilesional DLPFC in the PSD group, its predictive value for PSD was even lower than that of conventional clinical indicators.

Most importantly, this study identifies $PCI^{ST}$, a perturbation-based marker of cortical complexity, as a robust and independent predictor of PSD. $PCI^{ST}$ reduction was observed across stimulation sites and hemispheres, reflecting a network-level vulnerability that transcends focal lesion characteristics. These findings provide evidence in favor of the hypothesis that PSD arises from a collapse in thalamo-cortical integrative dynamics—disrupting the brain's capacity for reentrant processing and coherent network communication.

$PCI^{ST}$ proved feasible and reproducible under real-world stroke unit and ICU conditions, confirming its clinical applicability for early delirium risk stratification. Beyond prediction, $PCI^{ST}$ may also serve as a mechanistically grounded target for individualized neuromodulatory interventions. Future work should focus on simplifying the TMS–EEG pipeline for routine bedside use and testing whether $PCI^{ST}$-guided stimulation protocols can prevent cognitive deterioration in high-risk stroke patients.

Together, these results advance $PCI^{ST}$ from a theoretical construct to a translational tool—offering a novel avenue for precision medicine approaches to delirium prevention in acute neurocritical care.

# 5 Zusammenfassung

Delirium stellt eine häufige und schwerwiegende Komplikation in der Akutphase nach einem Schlaganfall dar, für deren Auftreten bislang jedoch verlässliche Prädiktoren fehlen. Zunehmende Evidenz deutet darauf hin, dass Störungen großskaliger Hirnnetzwerkdynamiken einen zentralen pathogenetischen Mechanismus darstellen. Die Kombination von transkranieller Magnetstimulation mit Elektroenzephalographie (TMS-EEG) eröffnet hierbei die Möglichkeit, kortikale Netzwerkreaktivität sowie die Komplexität kortikaler Antworten in vivo systematisch zu erfassen.

Im Rahmen der vorliegenden Arbeit wurde untersucht, inwieweit TMS-EEG-Parameter – insbesondere der schnelle Perturbational Complexity Index ($PCI^{ST}$), ein Maß für die Integration und Differenzierung kortikaler Antworten – geeignet sind, die Entwicklung eines post-stroke Deliriums vorherzusagen, wenn die Messungen innerhalb der ersten 48 Stunden nach Schlaganfallbeginn, jedoch noch vor Auftreten eines Deliriums, durchgeführt werden.

Es wurden prospektiv 34 Patientinnen und Patienten mit akutem Schlaganfall in die Studie eingeschlossen. Neben Ruhe-EEG-Aufzeichnungen erfolgten TMS-EEG-Messungen mit Stimulation des dorsolateralen präfrontalen Cortex (DLPFC) sowie des superioren Parietallobus (SPL) jeweils in der ipsi- und kontraläsionalen Hemisphäre. Das Auftreten eines Deliriums wurde im 8-Stunden-Rhythmus anhand der Intensive Care Delirium Screening Checklist (ICDSC) sowie der DSM-5-Kriterien erhoben. Aus den TMS-EEG-Antworten wurden $PCI^{ST}$ und die natürliche Frequenz berechnet; zusätzlich wurde die Spektralleistung des Ruhe-EEG analysiert. Die prädiktive Validität wurde mittels logistischer Regressionsanalysen, ROC-Analysen und Korrelationen mit klinischen und bildgebenden Parametern, einschließlich NIHSS und Läsionsvolumen, überprüft.

Insgesamt entwickelten 13 der 34 Patientinnen und Patienten (38 %) ein post-stroke Delirium. Die Betroffenen wiesen signifikant höhere NIHSS-Scores, größere Läsionsvolumina sowie eine erhöhte Theta-Band-Power im Ruhe-EEG auf, verglichen mit der Non-PSD-Gruppe. Diese Maße zeigten jedoch nur eine begrenzte Vorhersagekraft. Zwar wurde in der PSD-Gruppe eine Reduktion der natürlichen Frequenz des ipsiläsionalen DLPFC beobachtet, deren prädiktiver Wert lag jedoch unter dem klinischer Standardindikatoren.

Von zentraler Bedeutung ist der Befund, dass $PCI^{ST}$ als perturbationsbasierter Marker kortikaler Komplexität einen robusten und unabhängigen Prädiktor für

das Auftreten eines post-stroke Deliriums darstellt. Die Reduktion von $PCI^{ST}$ wurde unabhängig von Stimulationsort und Hemisphäre nachgewiesen, was auf eine netzwerkweite Vulnerabilität hinweist, die über die Charakteristika fokaler Läsionen hinausgeht. Diese Ergebnisse stützen die Annahme, dass PSD durch einen Zusammenbruch thalamo-kortikaler Integrationsdynamiken entsteht, wodurch die Fähigkeit des Gehirns zur rekurrenten Verarbeitung und kohärenten Netzwerkkommunikation beeinträchtigt wird.

Darüber hinaus konnte gezeigt werden, dass $PCI^{ST}$ auch unter den praktischen Bedingungen einer Stroke Unit bzw. Intensivstation zuverlässig und reproduzierbar bestimmbar ist. Damit wird die klinische Anwendbarkeit dieses Markers für eine frühzeitige Risikostratifizierung bestätigt. Über die reine Vorhersage hinaus erscheint $PCI^{ST}$ als vielversprechendes, mechanistisch fundiertes Ziel für individualisierte neuromodulatorische Interventionen. Zukünftige Studien sollten auf eine weitere Vereinfachung der TMS-EEG-Pipeline für den routinemäßigen Einsatz am Krankenbett abzielen sowie prüfen, ob $PCI^{ST}$-gesteuerte Stimulationsprotokolle die kognitive Verschlechterung bei Hochrisikopatienten verhindern können.

Zusammenfassend belegen die Ergebnisse, dass $PCI^{ST}$ von einem primär theoretischen Konzept zu einem translationalen Instrument weiterentwickelt werden konnte – und damit einen innovativen Ansatz für präzisionsmedizinische Strategien zur Prävention von Delirium in der akuten Schlaganfallbehandlung eröffnet.

# 6 Bibliography


ALVAREZ-PEREZ, F. J. & PAIVA, F. 2017. Prevalence and Risk Factors for Delirium in Acute Stroke Patients. A Retrospective 5-Years Clinical Series. *J Stroke Cerebrovasc Dis,* 26**,** 567-573.

ANGELIDIS, A., VAN DER DOES, W., SCHAKEL, L. & PUTMAN, P. 2016. Frontal EEG theta/beta ratio as an electrophysiological marker for attentional control and its test-retest reliability. *Biol Psychol,* 121**,** 49-52.

BAI, Y., BELARDINELLI, P., THOENNES, C., BLUM, C., BAUR, D., LAICHINGER, K., LINDIG, T., ZIEMANN, U. & MENGEL, A. 2023. Cortical reactivity to transcranial magnetic stimulation predicts risk of post-stroke delirium. *Clin Neurophysiol,* 148**,** 97-108.

BARR, J., FRASER, G. L., PUNTILLO, K., ELY, E. W., GÉLINAS, C., DASTA, J. F., DAVIDSON, J. E., DEVLIN, J. W., KRESS, J. P., JOFFE, A. M., COURSIN, D. B., HERR, D. L., TUNG, A., ROBINSON, B. R., FONTAINE, D. K., RAMSAY, M. A., RIKER, R. R., SESSLER, C. N., PUN, B., SKROBIK, Y. & JAESCHKE, R. 2013. Clinical practice guidelines for the management of pain, agitation, and delirium in adult patients in the intensive care unit. *Crit Care Med,* 41**,** 263-306.

BILEK, A. J. & RICHARDSON, D. 2023. Post-stroke delirium and challenges for the rehabilitation setting: A narrative review. *J Stroke Cerebrovasc Dis,* 32**,** 107149.

BLECK, T. P. 2018. Dopamine Antagonists in ICU Delirium. *N Engl J Med,* 379**,** 2569-2570.

BOUKRINA, O. & BARRETT, A. M. 2017. Disruption of the ascending arousal system and cortical attention networks in post-stroke delirium and spatial neglect. *Neurosci Biobehav Rev,* 83**,** 1-10.

BOUKRINA, O., KOWALCZYK, M., KOUSH, Y., KONG, Y. & BARRETT, A. M. 2022. Brain Network Dysfunction in Poststroke Delirium and Spatial Neglect: An fMRI Study. *Stroke,* 53**,** 930-938.

BRUNIA, C. H. 2001. Thalamo-cortical relations in attention and consciousness. *Int J Psychophysiol,* 43**,** 1-4.

CAO, K. X., MA, M. L., WANG, C. Z., IQBAL, J., SI, J. J., XUE, Y. X. & YANG, J. L. 2021. TMS-EEG: An emerging tool to study the neurophysiologic biomarkers of psychiatric disorders. *Neuropharmacology,* 197**,** 108574.

CAPILLA, A., ARANA, L., GARCÍA-HUÉSCAR, M., MELCÓN, M., GROSS, J. & CAMPO, P. 2022. The natural frequencies of the resting human brain: An MEG-based atlas. *Neuroimage,* 258**,** 119373.

CATANI, M. & THIEBAUT DE SCHOTTEN, M. 2008. A diffusion tensor imaging tractography atlas for virtual in vivo dissections. *Cortex,* 44**,** 1105-32.

CELLIER, D., RIDDLE, J., PETERSEN, I. & HWANG, K. 2021. The development of theta and alpha neural oscillations from ages 3 to 24 years. *Dev Cogn Neurosci,* 50**,** 100969.

CHEN, T. J., CHUNG, Y. W., CHANG, H. R., CHEN, P. Y., WU, C. R., HSIEH, S. H. & CHIU, H. Y. 2021. Diagnostic accuracy of the CAM-ICU and ICDSC in detecting intensive care unit delirium: A bivariate meta-analysis. *Int J Nurs Stud,* 113**,** 103782.

CHRISTOFF, K., IRVING, Z. C., FOX, K. C., SPRENG, R. N. & ANDREWS-HANNA, J. R. 2016. Mind-wandering as spontaneous thought: a dynamic framework. *Nat Rev Neurosci,* 17**,** 718-731.

COLE, M. W., REPOVŠ, G. & ANTICEVIC, A. 2014. The frontoparietal control system: a central role in mental health. *Neuroscientist,* 20**,** 652-64.

COLTHEART, M. 2007. Cognitive neuropsychiatry and delusional belief. *Q J Exp Psychol (Hove),* 60**,** 1041-62.

COMOLATTI, R., PIGORINI, A., CASAROTTO, S., FECCHIO, M., FARIA, G., SARASSO, S., ROSANOVA, M., GOSSERIES, O., BOLY, M., BODART, O., LEDOUX, D., BRICHANT, J. F., NOBILI, L., LAUREYS, S., TONONI, G., MASSIMINI, M. & CASALI, A. G. 2019. A fast and general method to empirically estimate the complexity of brain responses to transcranial and intracranial stimulations. *Brain Stimul,* 12**,** 1280-1289.

DA COSTA RODRIGUES, K., LEIVAS DE OLIVEIRA, R., DA SILVA CHAVES, J., ESTEVES DA ROCHA, V. M., FUZINATO DOS SANTOS, B., FRONZA, M. G., LUÍS DE CAMPOS DOMINGUES, N., SAVEGNAGO, L., WILHELM, E. A. & LUCHESE, C. 2022. A new arylsulfanyl-benzo-2,1,3-thiadiazoles derivative produces an anti-amnesic effect in mice by modulating acetylcholinesterase activity. *Chem Biol Interact,* 351**,** 109736.

DEVLIN, J. W., SKROBIK, Y., GÉLINAS, C., NEEDHAM, D. M., SLOOTER, A. J. C., PANDHARIPANDE, P. P., WATSON, P. L., WEINHOUSE, G. L., NUNNALLY, M. E., ROCHWERG, B., BALAS, M. C., VAN DEN BOOGAARD, M., BOSMA, K. J., BRUMMEL, N. E., CHANQUES, G., DENEHY, L., DROUOT, X., FRASER, G. L., HARRIS, J. E., JOFFE, A. M., KHO, M. E., KRESS, J. P., LANPHERE, J. A., MCKINLEY, S., NEUFELD, K. J., PISANI, M. A., PAYEN, J. F., PUN, B. T., PUNTILLO, K. A., RIKER, R. R., ROBINSON, B. R. H., SHEHABI, Y., SZUMITA, P. M., WINKELMAN, C., CENTOFANTI, J. E., PRICE, C., NIKAYIN, S., MISAK, C. J., FLOOD, P. D., KIEDROWSKI, K. & ALHAZZANI, W. 2018. Clinical Practice Guidelines for the Prevention and Management of Pain, Agitation/Sedation, Delirium, Immobility, and Sleep Disruption in Adult Patients in the ICU. *Crit Care Med,* 46**,** e825-e873.

EELES, E., BURIANOVA, H., PANDY, S. & PINSKER, D. 2017. Consciousness, Functional Networks and Delirium Screening. *Curr Aging Sci,* 10**,** 122-128.

FAIGLE, R., SUTTER, R. & KAPLAN, P. W. 2013. Electroencephalography of encephalopathy in patients with endocrine and metabolic disorders. *J Clin Neurophysiol,* 30**,** 505-16.

FAN, L., LI, H., ZHUO, J., ZHANG, Y., WANG, J., CHEN, L., YANG, Z., CHU, C., XIE, S., LAIRD, A. R., FOX, P. T., EICKHOFF, S. B., YU, C. & JIANG, T. 2016. The Human Brainnetome Atlas: A New Brain Atlas Based on Connectional Architecture. *Cereb Cortex,* 26**,** 3508-26.

FLEISCHMANN, R., TRAENKNER, S., KRAFT, A., SCHMIDT, S., SCHREIBER, S. J. & BRANDT, S. A. 2019. Delirium is associated with frequency band specific dysconnectivity in intrinsic connectivity networks: preliminary evidence from a large retrospective pilot case-control study. *Pilot Feasibility Stud,* 5**,** 2.

GERRANS, P. 2014. Pathologies of hyperfamiliarity in dreams, delusions and déjà vu. *Front Psychol,* 5**,** 97.

GÓMEZ-OCÁDIZ, R. & SILBERBERG, G. 2023. Corticostriatal pathways for bilateral sensorimotor functions. *Curr Opin Neurobiol,* 83**,** 102781.

GONG, X., JIN, S., ZHOU, Y., LAI, L. & WANG, W. 2024. Impact of delirium on acute stroke outcomes: A systematic review and meta-analysis. *Neurol Sci,* 45**,** 1897-1911.

GOSSERIES, O., SARASSO, S., CASAROTTO, S., BOLY, M., SCHNAKERS, C., NAPOLITANI, M., BRUNO, M. A., LEDOUX, D., TSHIBANDA, J. F., MASSIMINI, M., LAUREYS, S. & ROSANOVA, M. 2015. On the cerebral origin of EEG responses to TMS: insights from severe cortical lesions. *Brain Stimul,* 8**,** 142-9.

HANNA, A., JIRSCH, J., ALAIN, C., CORVINELLI, S. & LEE, J. S. 2023. Electroencephalogram measured functional connectivity for delirium detection: a systematic review. *Front Neurosci,* 17**,** 1274837.

HELFRICH, R. F., FIEBELKORN, I. C., SZCZEPANSKI, S. M., LIN, J. J., PARVIZI, J., KNIGHT, R. T. & KASTNER, S. 2018. Neural Mechanisms of Sustained Attention Are Rhythmic. *Neuron,* 99**,** 854-865.e5.

HERNANDEZ-PAVON, J. C., VENIERO, D., BERGMANN, T. O., BELARDINELLI, P., BORTOLETTO, M., CASAROTTO, S., CASULA, E. P., FARZAN, F., FECCHIO, M., JULKUNEN, P., KALLIONIEMI, E., LIOUMIS, P., METSOMAA, J., MINIUSSI, C., MUTANEN, T. P., ROCCHI, L., ROGASCH, N. C., SHAFI, M. M., SIEBNER, H. R., THUT, G., ZRENNER, C., ZIEMANN, U. & ILMONIEMI, R. J. 2023. TMS combined with EEG: Recommendations and open issues for data collection and analysis. *Brain Stimul,* 16**,** 567-593.

HERWEG, N. A., SOLOMON, E. A. & KAHANA, M. J. 2020. Theta Oscillations in Human Memory. *Trends Cogn Sci,* 24**,** 208-227.

HSHIEH, T. T., FONG, T. G., MARCANTONIO, E. R. & INOUYE, S. K. 2008. Cholinergic deficiency hypothesis in delirium: a synthesis of current evidence. *J Gerontol A Biol Sci Med Sci,* 63**,** 764-72.

INGVAR, D. H., SJÖLUND, B. & ARDÖ, A. 1976. Correlation between dominant EEG frequency, cerebral oxygen uptake and blood flow. *Electroencephalogr Clin Neurophysiol,* 41**,** 268-76.

JACOBSON, S. & JERRIER, H. 2000. EEG in delirium. *Semin Clin Neuropsychiatry,* 5**,** 86-92.

JULKUNEN, P., KIMISKIDIS, V. K. & BELARDINELLI, P. 2022. Bridging the gap: TMS-EEG from lab to clinic. *J Neurosci Methods,* 369**,** 109482.

KIM, J., PARK, S., KIM, K. N., HA, Y., SHIN, S. J., CHA, W., LEE, K. Y., CHOI, J. & KOO, B. N. 2023. Resting-state prefrontal EEG biomarker in correlation with postoperative delirium in elderly patients. *Front Aging Neurosci,* 15**,** 1224264.

KNEIHSL, M., BERGER, N., SUMERAUER, S., ASENBAUM-NAN, S., HÖGER, F. S., GATTRINGER, T., ENZINGER, C., AIGNER, M., FERRARI, J. & LANG, W. 2024. Management of delirium in acute stroke patients: a position paper by the Austrian Stroke Society on prevention, diagnosis, and treatment. *Ther Adv Neurol Disord,* 17**,** 17562864241258788.

LI, X., HONDA, S., NAKAJIMA, S., WADA, M., YOSHIDA, K., DASKALAKIS, Z. J., MIMURA, M. & NODA, Y. 2021. TMS-EEG Research to Elucidate the Pathophysiological Neural Bases in Patients with Schizophrenia: A Systematic Review. *J Pers Med,* 11.

LUTTENBACHER, I., PHILLIPS, A., KAZEMI, R., HADIPOUR, A. L., SANGHVI, I., MARTINEZ, J. & ADAMSON, M. M. 2022. Transdiagnostic role of glutamate and white matter damage in neuropsychiatric disorders: A Systematic Review. *J Psychiatr Res,* 147**,** 324-348.

MALDONADO, J. R. 2008. Delirium in the acute care setting: characteristics, diagnosis and treatment. *Crit Care Clin,* 24**,** 657-722, vii.

MALDONADO, J. R. 2013. Neuropathogenesis of delirium: review of current etiologic theories and common pathways. *Am J Geriatr Psychiatry,* 21**,** 1190-222.

MALDONADO, J. R. 2018. Delirium pathophysiology: An updated hypothesis of the etiology of acute brain failure. *Int J Geriatr Psychiatry,* 33**,** 1428-1457.

MATTISON, M. L. P. 2020. Delirium. *Ann Intern Med,* 173**,** ltc49-itc64.

MCMANUS, J., PATHANSALI, R., STEWART, R., MACDONALD, A. & JACKSON, S. 2007. Delirium post-stroke. *Age Ageing,* 36**,** 613-8.

MENGEL, A., ZURLOH, J., BOSSELMAN, C., BRENDEL, B., STADLER, V., SARTOR-PFEIFFER, J., MEISEL, A., FLEISCHMANN, R., ZIEMANN, U., POLI, S. & STEFANOU, M. I. 2021. Delirium REduction after administration of melatonin in acute ischemic stroke (DREAMS): A propensity score-matched analysis. *Eur J Neurol,* 28**,** 1958-1966.

MENON, V. & UDDIN, L. Q. 2010. Saliency, switching, attention and control: a network model of insula function. *Brain Struct Funct,* 214**,** 655-67.

MUKMININ, M. A., YEH, T. H., LIN, H. C., ROHMAH, I. & CHIU, H. Y. 2025. Global prevalence and risk factors of delirium among patients following acute stroke: A systematic review and meta-analysis. *J Stroke Cerebrovasc Dis,* 34**,** 108221.

MUTANEN, T. P., BIABANI, M., SARVAS, J., ILMONIEMI, R. J. & ROGASCH, N. C. 2020. Source-based artifact-rejection techniques available in TESA, an open-source TMS-EEG toolbox. *Brain Stimul,* 13**,** 1349-1351.

NARDONE, R., SEBASTIANELLI, L., VERSACE, V., FERRAZZOLI, D., SALTUARI, L. & TRINKA, E. 2021. TMS-EEG Co-Registration in Patients with Mild Cognitive Impairment, Alzheimer's Disease and Other Dementias: A Systematic Review. *Brain Sci,* 11.

OLDENBEUVING, A. W., DE KORT, P. L., JANSEN, B. P., ALGRA, A., KAPPELLE, L. J. & ROKS, G. 2011. Delirium in the acute phase after stroke: incidence, risk factors, and outcome. *Neurology,* 76**,** 993-9.

OLDENBEUVING, A. W., DE KORT, P. L., VAN ECK VAN DER SLUIJS, J. F., KAPPELLE, L. J. & ROKS, G. 2014. An early prediction of delirium in the acute phase after stroke. *J Neurol Neurosurg Psychiatry,* 85**,** 431-4.

PAPARELLA, I., VANDERWALLE, G., STAGG, C. J. & MAQUET, P. 2023. An integrated measure of GABA to characterize post-stroke plasticity. *Neuroimage Clin,* 39**,** 103463.

PUY, L., BARBAY, M., ROUSSEL, M., CANAPLE, S., LAMY, C., ARNOUX, A., LECLERCQ, C., MAS, J. L., TASSEEL-PONCHE, S., CONSTANS, J. M. & GODEFROY, O. 2018. Neuroimaging Determinants of Poststroke Cognitive Performance. *Stroke,* 49**,** 2666-2673.

REGAL, P. 2017. Delirium: a guide for the general physician. *Clin Med (Lond),* 17**,** 381.

RHEE, J. Y., COLMAN, M. A., MENDU, M., SHAH, S. J., FOX, M. D., ROST, N. S. & KIMCHI, E. Y. 2022. Associations Between Stroke Localization and Delirium: A Systematic Review and Meta-Analysis. *J Stroke Cerebrovasc Dis,* 31**,** 106270.

ROGASCH, N. C., SULLIVAN, C., THOMSON, R. H., ROSE, N. S., BAILEY, N. W., FITZGERALD, P. B., FARZAN, F. & HERNANDEZ-PAVON, J. C. 2017. Analysing concurrent transcranial magnetic stimulation and electroencephalographic data: A review and introduction to the open-source TESA software. *Neuroimage,* 147**,** 934-951.

ROSANOVA, M., CASALI, A., BELLINA, V., RESTA, F., MARIOTTI, M. & MASSIMINI, M. 2009. Natural frequencies of human corticothalamic circuits. *J Neurosci,* 29**,** 7679-85.

ROSSI, S., ANTAL, A., BESTMANN, S., BIKSON, M., BREWER, C., BROCKMÖLLER, J., CARPENTER, L. L., CINCOTTA, M., CHEN, R., DASKALAKIS, J. D., DI LAZZARO, V., FOX, M. D., GEORGE, M. S., GILBERT, D., KIMISKIDIS, V. K., KOCH, G., ILMONIEMI, R. J., LEFAUCHEUR, J. P., LEOCANI, L., LISANBY, S. H., MINIUSSI, C., PADBERG, F., PASCUAL-LEONE, A., PAULUS, W., PETERCHEV, A. V., QUARTARONE, A., ROTENBERG, A., ROTHWELL, J., ROSSINI, P. M., SANTARNECCHI, E., SHAFI, M. M., SIEBNER, H. R., UGAWA, Y., WASSERMANN, E. M., ZANGEN, A., ZIEMANN, U. & HALLETT, M. 2021. Safety and recommendations for TMS use in healthy subjects and

patient populations, with updates on training, ethical and regulatory issues: Expert Guidelines. *Clin Neurophysiol,* 132**,** 269-306.

ROSSINI, P. M., BURKE, D., CHEN, R., COHEN, L. G., DASKALAKIS, Z., DI IORIO, R., DI LAZZARO, V., FERRERI, F., FITZGERALD, P. B., GEORGE, M. S., HALLETT, M., LEFAUCHEUR, J. P., LANGGUTH, B., MATSUMOTO, H., MINIUSSI, C., NITSCHE, M. A., PASCUAL-LEONE, A., PAULUS, W., ROSSI, S., ROTHWELL, J. C., SIEBNER, H. R., UGAWA, Y., WALSH, V. & ZIEMANN, U. 2015. Non-invasive electrical and magnetic stimulation of the brain, spinal cord, roots and peripheral nerves: Basic principles and procedures for routine clinical and research application. An updated report from an I.F.C.N. Committee. *Clin Neurophysiol,* 126**,** 1071-1107.

SANDERS, R. D. 2011. Hypothesis for the pathophysiology of delirium: role of baseline brain network connectivity and changes in inhibitory tone. *Med Hypotheses,* 77**,** 140-3.

SARASSO, S., D'AMBROSIO, S., FECCHIO, M., CASAROTTO, S., VIGANÒ, A., LANDI, C., MATTAVELLI, G., GOSSERIES, O., QUARENGHI, M., LAUREYS, S., DEVALLE, G., ROSANOVA, M. & MASSIMINI, M. 2020. Local sleep-like cortical reactivity in the awake brain after focal injury. *Brain,* 143**,** 3672-3684.

SEIFERT, C. L., SCHÖNBACH, E. M., MAGON, S., GROSS, E., ZIMMER, C., FÖRSCHLER, A., TÖLLE, T. R., MÜHLAU, M., SPRENGER, T. & POPPERT, H. 2016. Headache in acute ischaemic stroke: a lesion mapping study. *Brain,* 139**,** 217-26.

SHAW, R. C., WALKER, G., ELLIOTT, E. & QUINN, T. J. 2019. Occurrence Rate of Delirium in Acute Stroke Settings: Systematic Review and Meta-Analysis. *Stroke,* 50**,** 3028-3036.

SHEPHERD, G. M. G. & YAMAWAKI, N. 2021. Untangling the cortico-thalamo-cortical loop: cellular pieces of a knotty circuit puzzle. *Nat Rev Neurosci,* 22**,** 389-406.

SIOKAS, V., FLEISCHMANN, R., FEIL, K., LIAMPAS, I., KOWARIK, M. C., BAI, Y., STEFANOU, M. I., POLI, S., ZIEMANN, U., DARDIOTIS, E. & MENGEL, A. 2022. The Role of Vascular Risk Factors in Post-Stroke Delirium: A Systematic Review and Meta-Analysis. *J Clin Med,* 11.

SMITH, C. J., HODGE, D., HARRISON, F. E. & WILLIAMS ROBERSON, S. 2024. The Pathophysiology and Biomarkers of Delirium. *Semin Neurol,* 44**,** 720-731.

SRIDHARAN, D., LEVITIN, D. J. & MENON, V. 2008. A critical role for the right fronto-insular cortex in switching between central-executive and default-mode networks. *Proc Natl Acad Sci U S A,* 105**,** 12569-74.

STOLLINGS, J. L., KOTFIS, K., CHANQUES, G., PUN, B. T., PANDHARIPANDE, P. P. & ELY, E. W. 2021. Delirium in critical illness: clinical manifestations, outcomes, and management. *Intensive Care Med,* 47**,** 1089-1103.

STRAFELLA, R., CHEN, R., RAJJI, T. K., BLUMBERGER, D. M. & VOINESKOS, D. 2022. Resting and TMS-EEG markers of treatment response in major depressive disorder: A systematic review. *Front Hum Neurosci,* 16**,** 940759.

SUN, M., LIU, M., ZHANG, F., SANG, L., SONG, Y., LI, P., LIU, S., YANG, H., MA, L., CAO, J., MI, W. & MA, Y. 2024. Triglyceride-glucose index predicts postoperative delirium in elderly patients with type 2 diabetes mellitus: a retrospective cohort study. *Lipids Health Dis,* 23**,** 107.

TREMBLAY, S., ROGASCH, N. C., PREMOLI, I., BLUMBERGER, D. M., CASAROTTO, S., CHEN, R., DI LAZZARO, V., FARZAN, F., FERRARELLI, F., FITZGERALD, P. B., HUI, J., ILMONIEMI, R. J., KIMISKIDIS, V. K., KUGIUMTZIS, D., LIOUMIS, P., PASCUAL-LEONE, A., PELLICCIARI, M. C., RAJJI, T., THUT, G., ZOMORRODI, R., ZIEMANN, U. & DASKALAKIS, Z. J. 2019. Clinical utility and prospective of TMS-EEG. *Clin Neurophysiol,* 130**,** 802-844.

TZOURIO-MAZOYER, N., LANDEAU, B., PAPATHANASSIOU, D., CRIVELLO, F., ETARD, O., DELCROIX, N., MAZOYER, B. & JOLIOT, M. 2002. Automated anatomical labeling of activations in SPM using a macroscopic anatomical parcellation of the MNI MRI single-subject brain. *Neuroimage,* 15**,** 273-89.

VALLESI, A., DEL FELICE, A., CAPIZZI, M., TAFURO, A., FORMAGGIO, E., BISIACCHI, P., MASIERO, S. & AMBROSINI, E. 2021. Natural oscillation frequencies in the two lateral prefrontal cortices induced by Transcranial Magnetic Stimulation. *Neuroimage,* 227**,** 117655.

VAN DELLEN, E., VAN DER KOOI, A. W., NUMAN, T., KOEK, H. L., KLIJN, F. A., BUIJSROGGE, M. P., STAM, C. J. & SLOOTER, A. J. 2014. Decreased functional connectivity and disturbed directionality of information flow in the electroencephalography of intensive care unit patients with delirium after cardiac surgery. *Anesthesiology,* 121**,** 328-35.

VAN MONTFORT, S. J. T., VAN DELLEN, E., STAM, C. J., AHMAD, A. H., MENTINK, L. J., KRAAN, C. W., ZALESKY, A. & SLOOTER, A. J. C. 2019. Brain network disintegration as a final common pathway for delirium: a systematic review and qualitative meta-analysis. *Neuroimage Clin,* 23**,** 101809.

VAN MONTFORT, S. J. T., VAN DELLEN, E., VAN DEN BOSCH, A. M. R., OTTE, W. M., SCHUTTE, M. J. L., CHOI, S. H., CHUNG, T. S., KYEONG, S., SLOOTER, A. J. C. & KIM, J. J. 2018. Resting-state fMRI reveals network disintegration during delirium. *Neuroimage Clin,* 20**,** 35-41.

WANG, Y., DANG, Y., BAI, Y., XIA, X. & LI, X. 2023. Evaluating the effect of spinal cord stimulation on patient with disorders of consciousness: A TMS-EEG study. *Comput Biol Med,* 166**,** 107547.

WANG, Y., NIU, Z., XIA, X., BAI, Y., LIANG, Z., HE, J. & LI, X. 2022. Application of Fast Perturbational Complexity Index to the Diagnosis and Prognosis

for Disorders of Consciousness. *IEEE Trans Neural Syst Rehabil Eng,* 30**,** 509-518.

WILCOX, M. E., GIRARD, T. D. & HOUGH, C. L. 2021. Delirium and long term cognition in critically ill patients. *Bmj,* 373**,** n1007.

WILLIAMS ROBERSON, S., AZEEZ, N. A., FULTON, J. N., ZHANG, K. C., LEE, A. X. T., YE, F., PANDHARIPANDE, P., BRUMMEL, N. E., PATEL, M. B. & ELY, E. W. 2023. Quantitative EEG signatures of delirium and coma in mechanically ventilated ICU patients. *Clin Neurophysiol,* 146**,** 40-48.

WILSON, J. E., MART, M. F., CUNNINGHAM, C., SHEHABI, Y., GIRARD, T. D., MACLULLICH, A. M. J., SLOOTER, A. J. C. & ELY, E. W. 2020. Delirium. *Nat Rev Dis Primers,* 6**,** 90.

XU, C., YUAN, Z., CHEN, Z., LIAO, Z., LI, S., FENG, Y., TANG, Z., NIAN, J., HUANG, X., ZHONG, H. & XIE, Q. 2024. Perturbational complexity index in assessing responsiveness to rTMS treatment in patients with disorders of consciousness: a cross-over randomized controlled trial study. *J Neuroeng Rehabil,* 21**,** 167.

YE, F., HO, M. H. & LEE, J. J. 2024. Prevalence of post-stroke delirium in acute settings: A systematic review and meta-analysis. *Int J Nurs Stud,* 154**,** 104750.

YOUNG, J. W. S. 2017. The network model of delirium. *Med Hypotheses,* 104**,** 80-85.

ZHANG, G. B., LI, H. Y., YU, W. J., YING, Y. Z., ZHENG, D., ZHANG, X. K., WANG, Y. G., SHI, G. Z. & HUANG, H. W. 2024a. Occurrence and risk factors for post-stroke delirium: A systematic review and meta-analysis. *Asian J Psychiatr,* 99**,** 104132.

ZHANG, G. B., LV, J. M., YU, W. J., LI, H. Y., WU, L., ZHANG, S. L., SHI, G. Z. & HUANG, H. W. 2024b. The associations of post-stroke delirium with outcomes: a systematic review and meta-analysis. *BMC Med,* 22**,** 470.

# 7 Declaration of Personal Contribution

The work was carried out at the University Hospital of Tübingen, Department of Neurology with a focus on neurovascular diseases, under the supervision of PD Dr. med. Annerose Mengel and Prof. Ulf Ziemann.

PD Dr. med. Annerose Mengel came up with the concept and idea for the study. She wrote the ethics application, submitted it to the ethics committee and supervised the project. She was responsible for patient recruitment and arranged the necessary imaging. Prof. Ulf Ziemann and PD Dr. med. Annerose Mengel were responsible for supervising the work carried out.

All experiments were performed by me, Gongfei Li, in collaboration with Frederick Straten. Frederick Straten was also responsible for the collection of all clinical data relevant to the test subjects. All the TMS-EEG data and MRI data processing and analysis were performed by myself.

The statistical analysis was performed independently by myself and supervised by PD Dr. Annerose Mengel.

I declare that I have written the manuscript independently and have not used any sources other than those cited.

# 8 Acknowledgements

I am deeply grateful to PD Dr. med. Annerose Mengel and Prof. Ulf Ziemann, for their invaluable guidance, patience, and inspiration throughout my doctoral journey. I would also like to thank my lab colleagues for their support and friendship, which made this work possible and enjoyable. My heartfelt thanks go to my family and girlfriend for their endless love and understanding, which have sustained me along the way. Finally, I gratefully acknowledge the support of the China Scholarship Council (CSC), which made my doctoral study abroad possible.